EUROfusion

EUROFUSION WPJET1–PR(15)39

A.E. Jaervinen et al.

Impact of Divertor Geometry on Radiative Divertor Performance in JET H-mode Plasmas

Preprint of Paper to be submitted for publication in
Plasma Physics and Controlled Fusion

This work has been carried out within the framework of the EUROfusion Consortium and has received funding from the Euratom research and training programme 2014-2018 under grant agreement No 633053. The views and opinions expressed herein do not necessarily reflect those of the European Commission.

Impact of divertor geometry on radiative divertor performance in JET H-mode plasmas

A. E. Jaervinen[1], S. Brezinsek[2], C. Giroud[3], M. Groth[1], C. Guillemaut[4], P. Belo[3], M. Brix[3], G. Corrigan[3], P. Drewelow[5], D. Harting[3], A. Huber[2], K.D. Lawson[3], B. Lipschultz[6], C.F. Maggi[3], G.F. Matthews[3], A.G. Meigs[3], D. Moulton[3], M.F. Stamp[3], S. Wiesen[2], and JET Contributors[1]

EUROfusion Consortium, JET, Culham Science Centre, Abingdon, OX14 3DB, UK.
[1] Aalto University, Espoo, Finland.
[2] Forschungszentrum Jülich GmbH, Institut für Energie- und Klimaforschung Plasmaphysik, 52425 Jülich, Germany.
[3] CCFE, Culham Science Centre, Abingdon, OX13 3DB, UK.
[4] Instituto de Plasmas e Fusão Nuclear, Instituto Superior Técnico, Universidade Lisboa, PT
[5] Max-Planck Institute for Plasma Physics, Greifswald, Germany.
[6] York Plasma Institute, University of York, Heslington, York YO10 5DD, UK.

e-mail: aaro.jarvinen@aalto.fi

Abstract

Radiative, partially detached divertor operation in JET H-mode plasmas with the ITER-like wall have been experimentally investigated and simulated with EDGE2D-EIRENE in horizontal and vertical LFS divertor configurations. The simulations show that the divertor heat fluxes at the low field side (LFS) can be reduced with N_2-injection in similar fashion in both configurations, qualitatively consistent with experimental observations. However, the simulations show no substantial difference between the two configurations in the reduction of the peak heat flux at the LFS divertor plate as a function of the divertor radiation, nitrogen concentration, or pedestal Z_{eff}. Consistently, experiments show similar divertor radiation and nitrogen injection levels for similar LFS peak heat flux reduction in both configurations. Nevertheless, the LFS strike point is predicted to detach at 20% lower separatrix density in the vertical than in the horizontal configuration. However, since the peak LFS heat flux in partial detachment in the vertical configurations is shifted towards the far scrape-off layer (SOL), the simulations predict no benefit in the reduction of LFS peak heat flux for a given upstream density in the vertical configuration relative to a horizontal one. Nevertheless, a factor of 2 reduction of deuterium ionization source inside the separatrix is observed in the simulations when changing to the vertical configuration, therefore, yielding a significant reduction of pedestal fuelling in the model. The simulations capture the experimentally observed particle and heat flux reduction at the LFS divertor plate in both configurations, only when adjusting the impurity injection rate to reproduce the measured levels of divertor radiation. However, when imposing the divertor radiation with nitrogen, the divertor D_α-emissions are underestimated by a factor of 2 – 5 indicating a short-fall in radiation by the fuel species. In the vertical configuration, the detachment process is experimentally measured and predicted by EDGE2D-EIRENE to start next to the strike point, extending towards the far SOL with increasing degree of detachment. In contrast, in the horizontal divertor geometry, the entire divertor particle flux profile is reduced uniformly with increasing degree of detachment both in the experiments and in the simulations. Therefore, a well-defined, partially detached state, as described in [Kallenbach_NF_2015], does not exist for the horizontal divertor configuration in the model.

Abstract word count: 364

[1] *See the appendix of F.Romanelli et al., 25th IAEA FEC, St. Petersburg, Russia, 2014.*

1. Introduction

Partial divertor detachment is foreseen necessary in ITER to reduce the heat loads on the plasma-facing components (PFCs) below 10 MW/m^2, while maintaining confined plasmas parameters consistent with the plasma performance goals [PIPB_NF_2007]. Utilizing the B2-Eirene code package, the ITER divertor is designed to reach strike point detachment under fusion burn conditions by employing the vertical divertor configuration with injection of radiating impurities, such as neon [Kukushking_FED_2011, Pacher_JNM_2009]. The vertical divertor geometry is predicted to facilitate neutral recycling towards the strike point, therefore, enhancing the ionisation near the separatrix and concomitantly the densities and volumetric power losses in this region [Loarte_PPCF_2001, Lipschultz_FST_2007]. As a result, strike point detachment is expected at lower upstream densities, impurity concentration levels, and radiative power levels in the vertical than in the horizontal divertor configuration, and the operational space between partially and fully detached conditions is expected to be wider in the vertical divertor configuration. However, although the impact of divertor geometry on the detachment characteristics is experimentally observed in Alcator C-mod [Lipschultz_FST_2007], ASDEX Upgrade [Schneider_JNM_1999], and JT-60U [Asakura_NF_1999], the initial experimental results from JET-Mk I divertor showed only little difference in the approach to detachment between the two configurations [Loarte_JNM_1997, Loarte_NF_1998]. Consistently, recent L-mode experiments in JET with the ITER-like wall configuration showed also only minor differences, of the order of 20%, in the approach to detachment between the two configurations [Groth_JNM_2015]. In contrast, multi-fluid modelling with EDGE2D-EIRENE [Simonini_CPP_1994, Reiter_JNM_1992, Wiesen_ITC_2006] showed a clear impact of the configuration on the divertor conditions in JET-ILW [Groth_JNM_2015]. It was hypothesized that gas recirculation within the divertor structure producing complicated ionisation patterns, as well as unaccounted plasma transport processes in the main SOL and divertor, masked some of the geometry effects in these studies. Furthermore, the more closed vertical divertor configuration is expected to provide enhanced confinement of neutrals in the divertor chamber. This is expected to reduce the neutral leakage to upstream and pedestal plasma and, as a result, reduce pedestal fuelling by divertor recycling relative to more open divertor configurations. Also the sub divertor pressure is expected to increase relative to more open divertor configurations and, therefore, facilitate pumping efficiency, as has been previously observed [Groth_JNM_2015, Loarte_PPCF_2002, Moulton_EPS_2015]. The pedestal fuelling and sud-divertor neutral pressures are coupled to each other, as was indicated by recent work extending EDGE2D-

EIRENE to model the sud-divertor structures in JET [Moulton_EPS_2015]. In JET L-mode simulations, in low density plasmas, the sud-divertor pressures were higher in vertical than in horizontal for a given LFS mid-plane separatrix electron density, $n_{e,\,sep,\,LFS\text{-}MP}$, due to reduced neutral leakage to pedestal plasma in the vertical configuration [Moulton_EPS_2015]. As a result, higher divertor recycling levels and sud-divertor neutral pressured were needed in the vertical configuration to reproduce the same $n_{e,\,sep,\,LFS\text{-}MP}$ as in the horizontal configuration.

In this contribution, these studies will be extended to investigate the effect of the divertor plasma configuration on the radiative divertor conditions in baseline high-confinement mode (H-mode) plasmas in the JET ITER-like wall [Matthews_PhysScr_2011] with nitrogen injection: 2.5MA/2.6–2.7T, $q_{95} \sim 3.2 - 3.4$, $P_{in} \sim 15 - 22$ MW, high triangularity ~ 0.4, [Giroud_PPCF_2015]. The investigated configurations refer to the high-triangularity, horizontal target (high-δ/HT), and the high-triangularity, vertical target (high-δ/VT) configurations presented in [Giroud_PPCF_2015]. For simplicity, these will be called just horizontal and vertical configuration in this paper. However, unlike in the original divertor configuration studies at JET [Loarte_NF_1998], in this study, the HFS divertor strike point is on the vertical target in both configurations, due to the requirements to maintain a high triangularity plasma shape. The deuterium was fuelled at the HFS divertor into the common SOL, and nitrogen was injected at the LFS target (Fig. 1). The nitrogen injection location is in the common SOL in the horizontal configuration and in the private flux region in the vertical configuration. In both configurations, approximately a single deuterium fuelling level was used throughout the nitrogen seeding scan: horizontal 2.6 – 3.1e22 e/s, JET pulse numbers (JPN) 82806/85406; vertical 2.1 – 2.3e22 e/s, JPN 85269. In the unseeded plasmas, these produce equal electron density and temperature profiles at the LFS mid-plane in both configurations within diagnostic resolution (Fig. 2a). 2 nitrogen injection levels on top of the base cases, imposing partially detached conditions at the LFS divertor plate, are investigated in this study: JPNs in horizontal configuration – mid-N_2/82812, high-N_2/85408; JPNs in vertical configuration mid-N_2/85272, high-N_2/85274. The medium nitrogen injection cases correspond to nitrogen injection levels of about 2.0 – 2.5e22 e/s and the high nitrogen injection cases to levels of about 3.5e22 e/s. The main diagnostics used to characterise the plasmas as well as the magnetic equilibria in this study are illustrated in the Fig. 1.

2. EDGE2D-EIRENE setup

EDGE2D-EIRENE was executed for steady-state, inter-ELM simulations for these discharges to validate the model for predictions of radiation distributions and divertor

conditions in horizontal and vertical divertor configurations. Furthermore, the simulations are used to assess hierarchy of the physics processes and the impact of the divertor geometry on the radiative divertor performance.

Analysis of the ELM frequencies indicate that, in most of the plasmas in this study, the steady-state inter-ELM assumption is expected to be justified from the SOL plasma point of view, since the average time between consecutive ELMs is longer, ~ 20 – 60 ms, than the characteristic SOL relaxation time $L_{connection}/c_s$ ~ about 1 ms (table 1). However, the time that it takes for the PFC material recycling properties to saturate between ELMs may be comparable to the inter-ELM time [Brezinsek_JNM_2014]. Furthermore, the relaxation time for the pedestal is expected to be comparable to the inter-ELM time, and, therefore, the time-evolution of the pedestal plasma may impact at least the power flowing through the separatrix, as well as the pedestal and main SOL density profiles. Also, in the highest nitrogen seeded plasmas in the vertical target configuration in this study, the validity of the steady-state assumption becomes marginal, since these plasma reach type-III like ELM frequencies of 70 Hz, which means that the mean time between ELMs is only about 14ms. Therefore, the ELM contribution in the inter-ELM divertor physics observations cannot be completely ruled out, even though the characteristic SOL evolution time is still shorter than the inter-ELM time in these plasmas.

The main boundary conditions in the simulations presented in this study are similar to those used in [Jaervinen_JNM_2014]. In the divertor chamber below the X-point, spatially constant cross-field transport parameters are used as specified in [Jaervinen_JNM_2014]. Identical particle diffusivities are used for all particle species. Since the heat conductivity profiles in the edge transport barrier are adjusted to reproduce the experimentally measured pedestal electron temperature profiles in the unseeded JET-ILW simulation in the horizontal configuration, thus input to the simulations, the simulations do not capture the experimentally observed increase of pedestal temperatures with nitrogen seeding in JET-ILW. The deuterium fuelling levels are adjusted individually for the two configurations to provide the same $n_{e,\,sep,\,LFS\text{-}MP}$ in the two configurations, as measured experimentally. After this step, the deuterium fuelling is kept fixed throughout the nitrogen seeding scans, as was done in the experiment. As a result, the $n_{e,\,sep,\,LFS\text{-}MP}$ is floating in the simulations. In this approach, it is basically assumed that although the model is not expected to capture the deuterium throughput details (injection and pumping) with the given set of pumping surfaces and pumping albedos, the relative discrepancy between the experiment and the model in the deuterium throughput does not change significantly during the nitrogen seeding scan. To investigate the sensitivity of the

model results to the assumption of floating $n_{e,\,sep,\,LFS\text{-}MP}$, seeding scans are also conducted assuming fixed $n_{e,\,sep,\,LFS\text{-}MP} = 4e19\ m^{-3}$.

The input power in the base case simulations in this study is set to 8 MW, as it was in [Jaervinen_JNM_2014]. Based on the power balance analysis for the investigated plasmas, this is around the lower boundary of the estimated ranges for most of the discharges, even when subtracting the rate of the change of the pedestal stored energy, dW_{ped}/dt, between the ELMs from the SOL loss power: $P_{SOL} = P_{LOSS} - dW_{ped}/dt$; $P_{LOSS} = P_{HEAT} - P_{RAD,\,CORE}$ (table 1). In this analysis, the P_{SOL} increases from about 8 MW in the unseeded plasmas to about 10 MW in the high seeding rate plasmas. Furthermore, the uncertainties in estimating the dW_{ped}/dt-term, especially in high frequency ELMing conditions with nitrogen seeding, yield to uncertainties as large as +/-5 MW, which are of the order of the estimated dW_{ped}/dt-term value itself. Therefore, including this term in the analysis might be a questionable approach within the given diagnostics resolution. In the lower frequency ELMing conditions, uncertainties of the order of 1 – 2 MW are typically obtained for the dW_{ped}/dt-term (table 1). If the dW_{ped}/dt-term is left out from the analysis, the resulting P_{LOSS} values to the SOL are of about 14 – 16 MW. Nevertheless, since the simulations conducted in this study turn out to reproduce the measured LFS divertor heat and particle fluxes, as well as, the measured divertor radiation levels in the seeded plasmas, the resulting heat flux entering the LFS divertor in the simulations is not expected to be strongly underestimated relative to the measured values. This might be a consequence of underestimated heat transport to the main chamber wall. Since this work is mainly about the radiative divertor performance in horizontal and vertical configurations, these simulations are expected to provide close enough representation of the experimental divertor heat flux, such that the comparison to the experiments and the interpretations remain meaningful.

Physical sputtering of beryllium as given by Eckstein et al. [Eckstein_sput_2007] are used in the simulations. ADAS 96 atomic rates are used for fuel and impurity species [ADAS reference]. Tungsten impurities are not included in the simulations, since the EDGE2D-EIRENE version used in these studies is able to simulate only 2 impurity species, which were chosen to be beryllium and nitrogen. The motivation to simulate beryllium instead of tungsten is that beryllium radiates mainly in the SOL, whereas tungsten radiates mainly inside the pedestal in the simulations. Therefore, tungsten contamination would only reduce the P_{SOL} in the simulations and is, therefore, implicitly included in the uncertainty of the used P_{SOL} value [Jaervinen_NF_2015]. In the experiments, tungsten accumulation in the central plasma was controlled with central ICRH heating [Giroud_PPCF_2015].

Nitrogen is assumed fully recycling in this study, whereas all the other impurities are assumed non-recycling. The full recycling assumption for nitrogen is an extreme case, since nitrogen is chemically active, forms ammonia and sticks to the wall material [Oberkofler_JNM_2013]. However, as was calculated for AUG in [Kallenbach_PPCF_2010], due to the high plasma flux on the divertor components, the divertor surfaces are expected to reach near to equilibrium nitrogen concentration in a few seconds of plasma time, such that the effective recycling coefficient of nitrogen on those surfaces will become close to 1, at least in consecutive discharges with nitrogen. Nitrogen molecules are not included in the model. Instead, nitrogen particles are injected as atoms. In previous investigations, the spreading impact of nitrogen molecule break-up on the density distribution of singly ionized nitrogen, by formation of fast Franck-Condon atoms, was found to be less than 5% [Jaervinen_JNM_2014]. Nitrogen injection levels are feedback controlled in the simulations to scan through the radiated power levels observed experimentally. Nitrogen radiation levels of 0, 3, 4, 5, 6, and 7 MW were considered for both configurations. In comparison to the 3 experimental levels, the 0, 3 and 6 MW cases are used to represent the unseeded, medium-N_2, and high-N_2 injection cases in both configurations, respectively. The simulations with 7 MW of nitrogen radiation evolved to a radiation-condensation formation inside the X-point in both configurations terminating the evolution of the plasma solution due to yet unidentified numerical reasons. Due to these reasons, these data points will not be included in the figures.

For neutral atoms and molecules, and impurity atoms, the Kotov-2008 EIRENE model is used in this study [Kotov_PPCF_2008]. At the divertor targets, standard Bohm-Chodura sonic to supersonic plasma flow is assumed and the sheath-heat transmission coefficients for electrons and ions are set to 4.5 and 2.5, respectively [Bohm, Chodura, Stangeby]. In these studies, cross-field drifts are omitted due to numerical stability issues that they impose. Due to these reasons, dedicated cross-field drift studies with EDGE2D-EIRENE are often conducted with carefully optimized grids and without impurities, as is done in [Chankin_PPCF_2015]. Ramping up the cases with cross-field drifts has not been successful by the time of writing this report. As a result, the simulations are expected not to be able to capture the experimentally observed HFS and LFS divertor conditions simultaneously. The impact of drifts is expected to be most significant in low- and high-recycling divertor conditions, and less significant in detached divertor conditions [AhoMantila_NF_2015, Groth_NF_2015].

An EDGE2D-EIRENE plasma solution is considered converged in this study if the simulation has reached an asymptotic state with the characteristic time-scales for the separatrix electron densities and temperatures at the LFS mid-plane, and the total particle,

energy, and impurity contents in the computational domain longer than 1s. Therefore, within characteristic inter-ELM time in the investigated plasmas, 20 – 50ms, these parameters evolve less than 5%.

The catalog folders of the EDGE2D-EIRENE plasma solutions investigated in this study are documented in the appendix of this paper.

3. Plasmas without impurity seeding

In the unseeded plasmas, the two divertor configurations reach similar main SOL and pedestal electron density and temperature profiles, as well as peak electron temperature at the LFS divertor plate (about 30 eV) (Figs. 2a, b). However, a factor of 2 higher peak saturation current is measured at the LFS plate in the vertical configuration than in the horizontal configuration, consistent with L-mode measurements in JET (Fig. 2c) [Groth_JNM_2015]. Furthermore, this may occur with a lower strike point electron temperature in the vertical configuration, although the divertor probe profiles do not properly resolve the vicinity of the strike point in this plasma. These observations would be inline with the conventional idea that the vertical configuration facilitates recycling towards the separatrix and, therefore, enhance the strike point densities and recycling levels and lower temperatures locally. However, the peak LFS target electron temperature is not reduced in the vertical configuration relative to the horizontal one. The electron temperature and saturation current just do not necessarily peak in the same spatial location in the vertical configuration, as they seem to be doing in the horizontal configuration. These findings provide confidence that although the impact of divertor geometry on the detachment characteristics and divertor profiles in JET has typically been observed to be significantly smaller than expected based on EDGE2D-EIRENE modelling [Loarte_JNM_1997, Loarte_NF_1998, Groth_JNM_2015], the qualitative impact of divertor geometry on the divertor recycling patterns and saturation current profiles is presumably credible. The electron temperature profiles do not agree with the measurements, at least in the far SOL (Fig. 2b). However, the measured particle fluxes in this region are small, and, as a result, the predicted electron temperature profiles in this region are very sensitive to small changes in the particle fluxes, assuming fixed power flux through the sheath. In other words, a factor of 2 increase in the predicted particle flux in the far SOL in the vertical geometry would be still within the scatter of the experimental probe data and would reduce the predicted electron temperature by a factor of 2. Therefore, it seems probable that the qualitative impact of divertor geometry on the divertor plasma characteristics is captured by the model, but the model presumably overestimates the effect. In fact, it would

not be surprising if the model overestimates the impact of divertor geometry, since the 2-D divertor fluid codes, as they stand, do not typically take into, at least,

(1) the detailed 3-D divertor structure with bypass leakages and neutral recirculation patterns,

(2) the scaling of the divertor and main chamber radial transport processes with plasma conditions (β, collisionality, SOL resistivity), and

(3) SOL fluctuations, intermittency of plasma transport and ELMs.

Even though these physics features are equally neglected in both configurations, it might be that the vertical configuration is more prone to enter such plasma conditions in the divertor, such as high collisionality close to the separatrix, that the impact of some of these features become significant in the overall divertor plasma solution. Moreover, the measured divertor characteristics are presumably sensitive to the exact location of the divertor strike point along the vertical target (divertor depth versus ionization mean-free path, strike point angle to the divertor tile, proximity of the strike point to the PFR floor and pump) as was documented in [Loarte_JNM_1997, Loarte_NF_1998]. However, recently, the impact of the location of the strike point on the detachment characteristic in vertical geometry in hydrogen L-mode plasmas in JET was found small [Groth_JNM_2015_2]. Also the plasma conditions (L-mode versus H-mode, heat-flux width, unseeded versus seeded) and PFC recycling properties (carbon versus tungsten) are likely to impact these characteristics. Probably due to these reasons, the qualitative impact on the divertor profiles is observed in this study as well as in [Huber_JNM_2013], but not in all of the previous studies in JET.

With the same base case boundary conditions and cross-field transport assumptions, and assuming the same electron density at the LFS mid-plane separatrix, the EDGE2D-EIRENE simulations reproduce the measured saturation currents and profiles at the LFS divertor target in the two configurations (Fig. 2c). As measured experimentally, EDGE2D-EIRENE predicts a factor of 2 – 3 higher LFS strike point saturation current in the vertical than in the horizontal divertor configuration. As a result, the strike point electron temperature is predicted to be about a factor of 3 lower in vertical than in the horizontal configuration (Fig. 2b). However, whereas in the horizontal divertor configuration the model reproduces the measured main SOL density profile, in the vertical configuration the density further than 0.5 cm away from the separatrix is underestimated by a factor of 2 (Fig. 2a). This flux surface is still well attached to the vertical plate, and, therefore, recycling on top of the baffle in the vicinity of the flux surface is not a likely explanation for this observation. This is associated with a factor of 2 – 3 overestimated far SOL electron temperatures in the vertical configuration (Fig. 2c).

The horizontal configuration is able to reach the factor of 2 higher far SOL densities relative to the vertical configuration for the same set of transport coefficients due to the broader divertor ionization distribution (Fig. 3). Whereas in the vertical configuration, the divertor ionization distribution is strongly localized in front of the strike point, the deuterium neutrals recycle towards the far SOL in horizontal configuration producing broader ionization distribution in front of the target. This strongly indicates that the vertical divertor simulations, as they stand, underestimate either the neutral leakage or the plasma transport into the far SOL. To investigate the impact of radial diffusivity on the predicted SOL density profile, the edge transport barrier diffusivity in the vertical divertor simulation was multiplied by a factor of 4. This increases the far SOL densities to levels only 20% below the lithium beam measurements. However, simultaneously the SOL heat flux width is increased to such high levels that the LFS divertor characteristics are not reproduced anymore. Also the pedestal density is reduced to 10% below the HRTS measurements. Nevertheless, it cannot be ruled out that conducting sensitivity scans with diffusive and convective radial transport in the ETB and far SOL, as well as by increasing the input power in the simulation, which would be very well justified due to the large uncertainties in the experimental P_{SOL}, that there would exist a set of boundary conditions, which would provide a simultaneous agreement for the main SOL and divertor profiles. In fact, it might well be the case that in this simulation, the power flowing into the SOL is underestimated relative to the experimental value, but due to underestimated radial transport the heat entering the narrow λ_q [Eich_PRL_2011] channel and, hence, the $q_{||}$ are in line with the experiments by coincidence. Nevertheless, the SOL characteristics in the narrow λ_q channel, which is the most interesting part of the SOL for power exhaust studies, are actually fairly well reproduced in the LFS SOL for the two configurations with only the simulation grid changed. Therefore, these cases provide a good base for the initial modelling studies of the impact of divertor geometry on the nitrogen radiation performance in these discharges.

In the plasmas without extrinsic impurity seeding, the predicted divertor radiation levels are underestimated by a factor of 2 when compared to the bolometer measurements (Fig. 4). In the HFS divertor leg, the underestimation is presumably partially explained by the omission of drifts in the simulations, since drifts would be expected to increase the HFS densities and radiation levels relative to the LFS divertor leg. However, inclusion of drifts is not expected to be sufficient to recover the experimentally measured radiated power levels in the partially detached HFS divertor, since divertor studies in partially detached and detached conditions with EDGE2D-EIRENE have typically shown a short-fall of deuterium radiation

also in the LFS divertor leg [Groth_NF_2013]. In the LFS divertor leg, the simulations reach the peak radiated power in the horizontal configuration, whereas the integral radiated power in the LFS divertor leg is still underestimated by about 30% (Fig. 4a). In the vertical configuration, the simulated LFS divertor leg radiation is about a factor of 2 lower than measured. However, one could argue that the vertical bolometer channels viewing the divertor do pick up radiation from the confined region, which is not modelled by EDGE2D-EIRENE. By subtracting the channels crossing the core, but not the divertor (channels at 270 degree line of sight in Fig. 4a) from the divertor viewing channels, the LFS divertor radiated power levels agree fairly well with the simulated values. However, such an approach is somewhat questionable since the horizontal bolometer channels crossing only the LFS SOL are still underestimated by the simulations by a factor of 2 (Fig. 4b). In both configurations, deuterium provides about 85 – 87% of the total predicted radiated power with beryllium providing the remaining 13 – 15%. Beryllium is not a very efficient radiator in the divertor electron temperatures in these plasmas. In [Jaervinen_NF_2015], sensitivity scans were conducted for the horizontal LFS target simulations by assuming full beryllium divertor, which is an extreme test case, in contrast with experimental observations showing practically pristine tungsten surfaces on both strike points [Widdowson_PhysScr_2014]. Even in these extreme cases, the beryllium radiation remained on the levels less than 20% of the deuterium radiation.

Similar to the radiated power, the overall LFS divertor D_α-emission is underestimated by a factor of 2 – 3 (Fig. 5). The peak LFS divertor D_α-emission is reproduced in the horizontal configuration for the location for which the line integrated radiated power is reproduced as well (Fig. 4a). This corresponds to the LFS strike point. Therefore, locally at the strike point in the horizontal configuration, the peak electron temperature, saturation current, radiated power, and D_α-emission are reproduced simultaneously by EDGE2D-EIRENE. This gives confidence that in attached conditions at the strike point ($T_e \sim 30$ eV), where the recycling deuterium is dominantly reflected back as atoms instead of molecules with tungsten PFCs (more than 70% recycled as atoms in EDGE2D-EIRENE [Jaervinen_NF_2015]), deuterium is the dominant divertor radiator in JET-ILW without extrinsic impurity seeding and the dominant D_α-emission channels (atomic D_α-emission in ionizing conditions) are included in the EDGE2D-EIRENE post processor. This is also consistent with L-mode plasma studies in JET [Groth_NF_2013, Lawson_JNM_2015] A possible explanation to why this does not hold for the vertical configuration is that the strike point is geometrically shadowed in this configuration, such that the line-integration might not be able to pick the peak radiation

location appropriately. In the HFS divertor leg the overall D_α-emission levels are underestimated by more than a factor of 5, which is presumably partially caused by omission of drifts, leading to overestimated electron temperature-density –ratios in the HFS divertor leg, underestimated recombination levels, and underestimated radiation. However, other unaccounted D_α-emission channels relevant for low temperature ($T_e < 2$ eV), high density ($n_e \sim 10^{20-21}$ m^{-3}) plasmas are expected to play a role as well. Furthermore, it is observed that the relative change in the shape of the divertor D_α-emission profile when changing from the horizontal to the vertical configuration is captured by the model qualitatively (Fig. 5). Vertical configuration is predicted and measured to emit more D_α in the HFS divertor leg and X-point, whereas stronger D_α-emission is predicted and measured for horizontal at the HFS baffle and LFS strike point.

4. Impact of the divertor geometry on the divertor radiation distribution and detachment characteristics

Within the scatter of the experimental data points and the range of the simulated EDGE2D-EIRENE cases in this study, the vertical divertor is not measured or predicted to offer any significant benefit in terms of minimizing the LFS divertor peak heat flux for a given radiation level imposed by nitrogen (Figs. 6a, b). Furthermore, the simulations predict no benefit in minimizing the plasma impurity contamination level and Z_{eff} for a given radiated power level. However, the latter prediction might not appropriately represent the experimental situation, where, in the horizontal configurations, the plasmas retained type-I ELM characteristics in nitrogen induced detachment whereas type-III ELM characteristics were observed in these conditions in the vertical configuration. As a result, the impurity transport characteristics in the vicinity of the pedestal are presumably not captured appropriately by these simulations neglecting ELMs altogether. Nevertheless, the simulations still indicate that, neglecting the ELM physics, the divertor geometry alone does not provide any benefit in maximising the radiative efficiency of impurities in the plasma, in contrast to expectations.

As can be observed, both vertical and horizontal divertor configurations in this study require a radiative fraction of about 50% to reach LFS divertor heat fluxes less than 2 MW/m^2, which is of the order of the diagnostics resolution of the divertor probes (Fig. 6a). Similarly, EDGE2D-EIRENE predicts that fairly similar SOL radiation fractions of 60 – 80% are needed in both configurations to reach LFS divertor peak heat fluxes less than 1 – 2 MW/m^2. The measured and simulated data points are not drawn in the same figure due to the

lack of a proper common x-axis between the experiment and the model. The EDGE2D-EIRENE simulations do not include the region inside $\rho \sim 0.9$, and therefore, the radiated power fraction cannot be used unambiguously. On the other hand, the P_{SOL} and P_{RAD}^{SOL} parameters are very challenging to be estimated experimentally for these ELMy H-mode plasmas, and, therefore, employing the P_{RAD}^{SOL}/P_{SOL} for the experimental data points would yield very large uncertainties. Nevertheless, the predicted and measured divertor bolometer channels for the high nitrogen injection cases are in good agreement, indicating that for these plasmas the model is presumably capturing the main features of the radiation distribution and absolute divertor radiation reasonably well (Fig. 9). Furthermore, it is observed that both in the experimental data set and in the model, the peak LFS heat flux is actually about a factor of 2 higher for vertical than for horizontal for similar radiation levels. In the EDGE2D-EIRENE model this is caused by less favourable inclination angle of the field line to the plate in the vertical than in the horizontal configuration, whereas the parallel heat fluxes towards the plate are very similar between the two configurations in the model. However, whereas in the horizontal configuration, the target heat flux peaks in the vicinity of the strike point throughout the seeding scan, in the vertical configuration, the strike point detaches early on in the seeding scan and the peak heat flux shifts towards the far SOL (Fig. 7). Furthermore, the vertical divertor offers no benefit in the model in minimizing the nitrogen concentration needed for a given radiated power level. The simulated average nitrogen concentration in the computational domain increases from about 0.7% to 2% in the seeding scan in the horizontal configuration and from about 1% to 3% in the seeding scan in the vertical configuration.

Since these simulations are conducted with floating $n_{e,\,sep,\,LFS\text{-}MP}$, the question remains whether this conclusion holds if the $n_{e,\,sep,\,LFS\text{-}MP}$ is kept fixed throughout the seeding scan. It turns out that for a fixed $n_{e,\,sep,\,LFS\text{-}MP}$, the vertical configuration outperforms horizontal one in the simulations (Fig. 8a). In the simulations, the horizontal configuration retains the $n_{e,\,sep,\,LFS\text{-}MP}$ throughout the seeding scan, whereas in the vertical configuration the $n_{e,\,sep,\,LFS\text{-}MP}$ is reduced nearly linearly from 4e19 m^{-3} to 2.6e19 m^{-3} within the seeding scan. However, this reduction is within the scatter of the experimental data. Nevertheless, to address this uncertainty, simulations with $n_{e,\,sep,\,LFS\text{-}MP}$ fixed to 4e19 m^{-3} with deuterium feedback control were conducted. In these simulations, the vertical divertor reaches LFS divertor peak heat fluxes less than 1MW/m^2 at 25% lower $P_{RAD,SOL}/P_{SOL}$ than the horizontal configuration (Fig. 8a). To maintain the same $n_{e,\,sep,\,LFS\text{-}MP}$ at these radiation levels where the LFS plasma reaches partial detachment, the deuterium puff in the simulations is increased by a factor of 4 relative

to the unseeded base case. In the experiment, a fixed deuterium puff level is used throughout the seeding scan investigated in this paper.

Furthermore, unseeded density scans were conducted, which also show little difference in the reduction of the peak LFS target heat flux with increasing $n_{e,\,sep,\,LFS\text{-}MP}$ between the two configurations (Fig. 8b). The vertical divertor does enter strike point detachment at 20% lower $n_{e,\,sep,\,LFS\text{-}MP}$ than the horizontal configuration. However, the peak LFS target heat flux, which is shifted towards far SOL in partial detachment in the vertical geometry, remains still comparable or higher to the strike point value in the horizontal configuration (Fig. 8b).

For the base case simulations with floating $n_{e,\,sep,\,LFS\text{-}MP}$, the simulations predict normalized divertor power spreading parameters S/f_x consistent with previous studied [Scarabosio_JNM_2015]. To estimate the predicted divertor power spreading parameters in these simulations, the target heat flux profiles, parameterized as in the equation (2) in [Eich_PRL_2011], were fitted to the predicted LFS divertor heat flux profiles, as was done in [Scarabosio_JNM_2015] (Fig. 7). Similar to SOLPS simulations for AUG in [Scarabosio_JNM_2015], also in this study, a factor of at least 2 – 3 higher S/f_x values are obtained in the vertical configuration than in the horizontal configuration (Fig. 7). Based on the Fig. 7 in [Scarabosio_JNM_2015], and the predicted $T_{e,sep,\,LFS,\,DIV}$ values in these simulations (Horizontal, 30 eV, 7.5 eV, and 0.5 eV; Vertical, 6.3 eV, 1.6 eV, 0.6 eV), the expected S/f_x-values are about 0.8 mm, 1.5 mm, and more than 2 mm in the horizontal, and 1.5 mm, 2 mm, and more than 2 mm in the vertical divertor simulations, respectively. The fits conducted for the 3 radiation levels in each configuration yield 0.82 mm, 0.71 mm, and 2.73 mm in the horizontal configuration, and 1.82 mm, 4.12 mm, and 19.6 mm in the vertical configuration, which are well in line with the Fig. 7 in [Scarabosio_JNM_2015].

Whereas in the unseeded plasmas, the divertor radiation is underestimated by a factor 2 in the EDGE2D-EIRENE simulations, by imposing the divertor radiation with nitrogen seeding, the measured radiated power levels and distribution in the divertor can be reproduced numerically in both configurations (Figs. 9, 10). It is observed that at the medium nitrogen injection level, in horizontal configuration the simulations capture the measured radiated power levels in the both divertor legs, whereas the radiated power in the X-point is still lower than measured. The missing X-point radiation is recovered in the simulations when increasing the nitrogen seeding further to impose LFS detachment, as is the case at the highest nitrogen injection rate. However, at the medium nitrogen injection case, the LFS conditions in the experiment are still high recycling, while there is considerable radiation at the X-point level already. This formation is not observed in the simulations, which require LFS detachment for

the radiation front to shift to the X-point to reproduce the measured levels of radiation there. Possible explanations for this discrepancy are omission of intermittency, fluctuations and ELMs in the simulations. However, in H-mode plasmas, the SOL is expected to be more quiescent between ELMs than in L-mode plasmas, as consequence of reduced transport in the vicinity of the pedestal. Therefore, intermittent transport between ELMs might not play such a role in the inter-ELM observations as it may in L-mode SOL characteristics. Also the omission of cross-field drifts might play a role, if in these high recycling conditions the pre-sheath electric potential gradient is still strong enough to drive significant particle flux from the LFS divertor leg into the private flux region thereby increasing the radiation levels below the X-point [Chankin_PPCF_2015]. Incidentally, when repeating the same exercise for the vertical divertor configuration, the simulations capture the measured radiation levels and distribution in the divertor for both medium and high nitrogen injection plasmas (Fig. 9).

The radiation distribution with nitrogen in the simulations follows the 10 – 30 eV electron temperature contour in the simulations, since this is the region where nitrogen is the most efficient radiator (Figs. 10, 11). In both configurations, more than 90% of the total radiation in computational domain occurs outside the separatrix until a MARFE-like, radiation condensation formation is formed inside the X-point. Once this formation is present, most of the radiation occurs inside the separatrix in the simulations. However, the simulations with this formation do not reach a state satisfying the convergence criterion in this study due to numerical difficulties occurring in the simulations once the formation turns on. Therefore, these simulation results may not fully represent an accurate solution for the equations in question. The bottom-line is that due to the radiative characteristics of nitrogen, nitrogen radiation is confined in the region where the plasma electron temperature increases from low values (less than 5 eV) to about 30 eV, which corresponds to the divertor chamber between target and X-point in JET in high-recycling to partially detached conditions (Figs. 10, 11). To which extend cross-field drifts change this picture by increasing the HFS divertor degree of detachment and nitrogen penetration and cooling of the X-point in conditions where the LFS divertor is still high-recycling or partially detached is still an open question. However, since these EDGE2D-EIRENE simulations, with impurity seeding levels feedback controlled to reproduce the measured levels of radiation, do actually capture the experimentally measured radiation distribution of the divertor bolometer channels fairly well without the need to include drift effects, the cross-field drifts might not just play a big role in these observations. This would also be consistent with previous findings in L-mode plasmas [AhoMantila_NF_2015], where it was observed that in low divertor temperature operation,

the necessary electric fields to drive considerable **E**x**B**-flows does not exist anymore. This can be checked for these cases by turning the drifts and currents on in EDGE2D-EIRENE. However, by the time of writing this report, the attempts to turn drifts on for these cases have not been successful, due to convergence issues.

The measured reduction of the LFS target electron temperatures, heat and particle fluxes in the detachment assisted by nitrogen is captured by the EDGE2D-EIRENE simulations in both configuration when imposing the measured levels of divertor radiation with nitrogen seeding (Fig. 11). In the simulations, in the horizontal configuration, the detachment assisted by nitrogen leads to reduction of the LFS saturation current across the entire profile. On the other hand, in the vertical configuration, strike point detaches first and the peak saturation current shifts towards far SOL with increasing degree of detachment (Fig. 11). These observations are also consistent with the LFS target Langmuir Probe measurements within the scatter of the data.

In the simulations of the horizontal LFS divertor configuration, the LFS strike point recycling levels increase first and the far SOL recycling levels drop when increasing the nitrogen seeding from the unseeded levels to the medium seeding level (Fig. 11b). This is caused by cooling of the far SOL plasma, whereas the strike point temperatures remain still around 10 eV. As a result, the broad ionization distribution in front the horizontal target contracts from the far SOL towards the strike point, where the plasma conditions are still ionizing. This increases the ionization source at the strike point and reduces it in the far SOL explaining the observed change in the saturation current profile. When increasing the nitrogen seeding further, also the strike point electron temperature collapses to low values below 1 eV, producing completely collapsed target electron temperature profiles. As a result, the ionization front detaches from the strike point and shifts towards the X-point producing a 'V-like' 2-D ionization profile in the divertor leg, which follows the 5 – 15 eV electron temperature contour (Fig. 12). As this happens, the saturation current profile at the LFS target is reduced uniformly across the profile. In other words, a well-defined, partially detached state, as described in [Kallenbach_NF_2015], does not exist for the horizontal configuration in these simulations, but, instead, a gradual, complete, divertor profile detachment follows the high-recycling divertor regime.

In the vertical configuration, neutral recycling occurs preferentially towards the separatrix and the private flux region, where the neutrals recycle on the divertor floor tiles, such as JET tile-5, and return towards the strike point at tile-7. Therefore, the main neutral reservoir in the divertor plasma in the vertical configuration is in the private flux region, whereas in the

horizontal configuration both PFR and far SOL provide neutral reservoir for deuterium ionization. As a result, unlike in the horizontal configuration, the divertor ionization is strongly localized close to the separatrix in the vertical configuration in the model, producing strong peak saturation currents close to the strike point in attached conditions in the vertical geometry (Figs. 12, 13). With moderate nitrogen injection, the divertor plasma cools down preferentially along the separatrix in the divertor leg, where the product of electron and nitrogen densities and radiative potential (electron temperature) are most favourable for nitrogen radiation (Figs. 10, 11). As this happens, the ionizing plasma contour (T_e > 5 eV) shifts towards far SOL, and neutrals penetrate radially further into the divertor leg increasing the saturation current away from the strike point relative to the attached base case values (Figs. 11, 12). Furthermore, the increased neutral density and momentum losses along the separatrix due to neutral friction as well as due cross-field diffusion and viscosity limit the parallel particle flow to the target, which would otherwise increase with reducing divertor electron temperatures. These two effects together provide the conventional partial detachment characteristics in the model, where the strike point detaches first and the peak saturation current shifts towards the far SOL. The same mechanism applies to the cases with increasing degree of detachment until the ionization front has propagated through the SOL and starts shifting towards the X-point producing completely detached divertor profiles. However, in the vertical divertor simulations, these completely detached profiles are only observed in the simulations entering the radiation-condensation formation inside X-point, as was also observed in recent SOLPS 5.0 simulations N_2-seeded H-mode plasmas in ASDEX Upgrade [Reimold_JNM_2015].

As was the case in the unseeded reference simulations, also in the seeded plasmas the divertor D_α-emission is underestimated by a factor 2 – 5, indicating a short-fall in radiation by the fuel species (Fig. 14). In the horizontal configuration, a factor of 2 – 5 increase of D_α-emission is observed experimentally in the LFS divertor leg between the X-point and the strike point with mid- to high-N_2 injection relative to the unseeded reference plasma (Fig. 14a, R-coord. 2.6 – 2.8). This is presumably caused by elongation of the deuterium ionization front upwards in the divertor leg towards the X-point. In the simulations, this increase is not observed in the medium nitrogen injection case, since this simulation retains still in attached, high-recycling conditions at the LFS plate, and most of the ionization occurs in front the strike point (Figs. 13, 14a). However, at the high nitrogen injection level case, a factor of 5 increase in the D_α-emission close to the LFS X-point is observer, which is still, however, a

factor of 3 – 4 below the experimental level (Fig. 14a). In these simulations, the increased D_α-emission close to the LFS X-point is caused by a shift of the deuterium ionization front into this region with the LFS divertor detachment such that excitation D_α-emission becomes significant in this region. In front of the strike point, the D_α-emission remains high or even increases relative to the unseeded base case simulation due to the onset of recombination D_α-emission in this region. In fact, the excitation and recombination D_α-emission form two distinct zones in the divertor leg in the simulation, following the electron temperature contour of the divertor plasma (excitation at T_e about 5 eV or above, recombination at T_e about 1 eV or below). In the vertical configuration, increase in the LFS D_α-emission with nitrogen seeding is also experimentally observed, although in this configuration the increase is seen throughout the divertor leg in contrast to the localized increase close to the LFS X-point in the horizontal configuration (Fig. 14). This difference between the D_α-emission distributions might stem from the vertical divertors tendency to retain the ionization front attached to the target in the far SOL even in conditions where the front extends close to the X-point already. In such conditions, the D_α-emission in the divertor leg could increase due to the elongation of the deuterium ionization front. The target levels, on the other hand, could increase both due to recombination emission from the strike point region as well as due to ionization emission from the far SOL region, which would be picked up by the same line of sight. However, the simulations do not show any significant change in the LFS divertor D_α-emission in this configuration with increasing nitrogen seeding. In the HFS divertor, D_α-emission is underestimated by a factor of 5 – 10 in both configurations. Whereas in the unseeded cases one could argue that the omission of drifts can partially explain the discrepancy, the role of drifts is expected to be less significant in the high seeding rate, detached plasmas. Therefore, the omission of drifts is not likely to fully explain the discrepancy in the HFS divertor. Instead, some D_α-emission channels, significant in low temperature (< 2 eV), high density (1e20 – 21 m^{-3}) plasmas, might not be properly taken into account in the EDGE2D-EIRENE post processing routine. Furthermore, due to the strong radiation-temperature –coupling for deuterium in low temperatures where the relevant reaction rates become very non-linear, the radiation short-fall with deuterium, as it stands, might be a consequence of the given fluid model not solving the physics details in the deuterium recycling region properly yet, leading to underestimated deuterium radiated power and D_α-emission as a symptom. In the detachment simulations with extrinsic impurities, as in this study, this does not necessarily lead to issues in reproducing the main features of detachment, since in this case, the deuterium

recycling is not the main power dissipation channel in the system. In plasmas without strong extrinsic impurity radiator present, the deuterium recycling must provide a divertor solution in detachment, which simultaneously satisfies particle, momentum and power conservation. Reaching detached solutions in the simulations without extrinsic impurities requires therefore reproduction of the delicate balance between ionization, power radiation, momentum loss processes, and recombination for deuterium, all of which depend strongly on the local electron temperature and density. In the simulations with extrinsic seeding, the power dissipation is mainly accomplished via the impurities, and the only requirement for deuterium to enable detachment is to provide sufficient momentum losses to prevent plasma flux runaway to the targets with reducing target electron temperatures as well as to limit neutral deuterium flow into the ionization region to provide particle balance in the divertor. Hence, the extrinsic impurity radiator takes one constraining equation (power balance) out of the set of equations needed to solve, which enables sufficient degrees of freedom to the system, such that detachment can be imposed even if the solver might not fully capture the physics details with deuterium exactly. Detachment simulations without extrinsic impurities is a much more delicate process and needs to be addressed in separate publications.

5. Impact of divertor geometry on the separatrix density and pedestal fuelling in nitrogen seeded H-mode plasmas in JET

With increasing nitrogen injection rate in the horizontal configuration, 25% increase of the pedestal electron density is experimentally observed at medium N_2-levels, followed by about 10% reduction at the high N_2-levels relative to the medium levels once the LFS divertor detachment is reached (Fig. 15a) [also C. Giroud, PPCF 2015]. In contrast, in the vertical configuration, a few % reduction of pedestal density is observed with increasing nitrogen seeding rate from the unseeded levels to partial LFS detachment. Interestingly, EDGE2D-EIRENE simulations reproduce this behaviour qualitatively, such that increasing only the nitrogen seeding rate relative to the unseeded base case, without changing any cross-field transport assumptions, monotonic 43% increase of pedestal electron density is obtained through the seeding scan in the horizontal configuration, whereas the pedestal electron density remains constant within 6% throughout the seeding scan in the vertical configuration (Fig. 15b). The reduction of pedestal electron density in the horizontal configurations following the LFS divertor detachment is not observed in the simulations and is presumably related to increase in the pedestal cross-field transport with LFS detachment or increasing upstream collisionality, not taken into account in this model.

These simulations do not match the pedestal electron temperature in the nitrogen seeded cases, since the pedestal performance is improved with nitrogen seeding in the experiment [Giroud_PPCF_2014], which does not occur in the model. Nevertheless, to investigate the sensitivity of the predicted pedestal temperature on the assumption of cross-field heat conductivity, the horizontal target simulation with 3 MW of nitrogen radiation was conducted with a factor of two reduced pedestal radial heat conductivity inside the separatrix. This change is sufficient to approximately reproduce the experimentally observed pedestal temperature increase with nitrogen and does not change the predicted pedestal density at all. Therefore, not matching the pedestal temperatures inside the separatrix is not expected to have any significant impact on the pedestal density predictions in these studies. Hence, to keep the simulations tractable, only 1 parameter (nitrogen seeding) is changed in the scan. Any assumption for scaling of the cross-field transport as a function of nitrogen content in the plasma, for example, would be a next level of sophistication, which cannot be properly understood unless the linear studies are conducted first. In other words, the edge fluid codes do not predict pedestal by definition, but they can provide understanding about the divertor neutral leakage and pedestal fuelling as well as LSF mid-plane separatrix densities and temperatures that are consistent with measured divertor quantities. Since the cross-field transport is only diffusive in the model, assuming the same diffusion coefficient for all the simulations in the scan, the pedestal density is determined by the pedestal deuterium ionization profile and poloidal separatrix electron density profiles, such that the diffusive out-flux of plasma given by the density gradient ($\sim n_{e,ped} - n_{e,sep}$) is balanced by the pedestal ionization source.

In the unseeded basecase, the two configurations reach the same electron density at the LFS mid-plane separatrix, but the total deuterium ionization source is about 40% lower in the vertical than in the horizontal configuration due to the enhanced screening of the divertor neutrals in the vertical configuration in the model (Figs. 15, 16a). As a result, the predicted pedestal electron density is about 15% lower in the vertical configuration (Fig. 15b). The experimentally measured electron density profiles at the LFS mid-plane are on top of each other in the two configurations (Fig. 2). Hence, the pedestal ionization might be underestimated by about 10 – 15% in these simulations and/or some of the relevant cross-field transport processes might be neglected in these simulations.

With increasing nitrogen injection rate and SOL radiation, an increase in the pedestal neutral fuelling is observed in both configurations (Figs. 15c, 16). However, in the horizontal configuration this is associated with approximately constant total pressure and electron

density at the LFS mid-plane separatrix, such that the pedestal density is increased with increasing pedestal fuelling (Fig. 15d). In the vertical configuration, on the other hand, the total pressure and electron density are reduced at the LFS mid-plane separatrix with increasing nitrogen injection such that, despite the increasing pedestal fuelling, the pedestal density does not increase in the model. This is presumably caused by detachment of the strike point region in the vertical target simulations at lower impurity and radiation levels than in the horizontal configuration, as is illustrated by the strong reduction of total pressure at the strike point at 40% SOL radiation fraction (Fig. 15d). As the strike point region detaches, the total pressure in the separatrix field line is reduced in the simulations, even though the power crossing the separatrix remains practically the same. In principle, this mechanism should reproduce the reduction of pedestal density in LFS detachment in the horizontal configuration as well. However, in the simulations, such a strong reduction of LFS mid-plane pressure in LFS detachment, as is observed in the vertical configuration, is not observed in the horizontal configuration.

The predicted poloidal neutral deuterium flux crossing the separatrix is about a factor of 2 higher around the LFS baffle in the horizontal configuration than in the vertical configuration in the unseeded and medium-N_2 injection cases in the simulations (Fig. 16). In the simulations representing the high-N_2 plasmas, the neutral flux to pedestal close to the LFS baffle is about a factor of 4 – 6 higher in horizontal than in the vertical configuration. This qualitative difference is caused by the direction of recycling neutrals in the divertor. In the horizontal configuration, neutrals are reflected towards the far SOL, and, as a result, form a neutral deuterium reservoir, which fuels the pedestal close to the LFS baffle. With increasing nitrogen seeding, the SOL in this region becomes more transparent to neutrals and the flux crossing the separatrix is strongly enhanced close to the LFS baffle. In the vertical configuration, on the other hand, the neutrals are preferentially recycling towards the PFR, and, therefore, such a strong LFS fuelling is not observed as in the horizontal configuration. Since these simulations do not include cross-field drifts and currents, the HFS/LFS divertor asymmetries are presumably underestimated, at least in the low radiative fraction plasmas. Therefore, the contribution of LFS fuelling relative to HFS fuelling, in the fuelling profiles might be overestimated. This same issue hinges also on the predicted pedestal densities.

6. Conclusions

Radiative divertor operation in nitrogen seeded, high-triangularity JET H-mode plasmas have been experimentally investigated and simulated with EDGE2D-EIRENE in horizontal

and vertical LFS divertor configurations. The simulations show no substantial difference between the two configurations in the reduction of the peak heat flux at the LFS divertor plate as a function of the divertor radiation, consistent with experimental observations. Furthermore, predicted unseeded density scans show no benefit in vertical configuration in minimizing the LFS peak heat flux for a given $n_{e,\,sep,\,LFS\text{-}MP}$. However, assuming fixed $n_{e,\,sep,\,LFS\text{-}MP}$ for a nitrogen seeding scan, the vertical configuration reaches LFS peak heat fluxes less than 1 MW/m^2 at about 25% lower SOL radiation values than the horizontal one. Therefore, if actively controlling the SOL density by increasing the deuterium puffing levels in the simulations with partial detachment, the vertical divertor is predicted to outperform the horizontal one in terms of needed radiation leves for a given reduction of LFS peak heat flux.

For the base case simulations with floating $n_{e,\,sep,\,LFS\text{-}MP}$, the simulations show no benefit in vertical configuration in minimizing the impurity contamination, fuel dilution, and Z_{eff} levels needed for a given radiated power level. However, a factor of 2 reduction of deuterium ionization source inside the separatrix is observed in the simulations when changing to the vertical configuration, therefore, yielding a significant reduction of pedestal fuelling in the model. Coupled with the reduction of the mid-plane separatrix pressure in the model with partial divertor detachment in the vertical configuration, the simulations do then reproduce qualitatively the experimentally observed trend of increasing pedestal density with nitrogen seeding in the horizontal configuration, but reduction of the pedestal density with seeding in the vertical configuration.

In the unseeded plasmas, for similar LFS mid-plane electron density and temperature profiles, the vertical configuration is measured to reach a factor of 2 higher peak saturation current at the LFS divertor plate, which is presumably associated with a lower strike point electron temperature than in the horizontal configuration. Assuming the same cross-field transport coefficients and LFS mid-plane electron densities in the model for the two configurations, the model captures the measured particle fluxes and their profiles at the LFS divertor plate. However, the far SOL electron density is underestimated by a factor of 2 in the vertical configuration but not in the horizontal configuration. This is presumably caused by underestimated ionization sources in the far SOL as well as unaccounted transport processes in the model in the vertical configuration. Furthermore, similar to earlier observations, the simulations underestimated the divertor radiation by a factor of 2.

With nitrogen seeding, both configurations reach detached conditions at the LFS plate in the experiment. When imposing the measured levels of divertor radiation with nitrogen seeding, the measured reduction of the LFS divertor saturation currents are captured by the

EDGE2D-EIRENE simulations in both configurations. However, when imposing the divertor radiation with nitrogen, the divertor D_α-emissions are still underestimated by a factor of 2 – 5 indicating a short-fall in radiation by the fuel species in detached conditions. In the horizontal configuration, the LFS saturation current profile is predicted to be reduced uniformly along the target with increasing degree of detachment. Therefore, a well-defined, partially detached state does not exist for the horizontal divertor configuration in the model. Instead, the divertor evolves from high-recycling conditions to a gradual complete divertor profile detachment. In the vertical configuration, on the other hand, the strike point detaches first, and the peak saturation current shifts towards the far SOL with increasing degree of detachment. These detachment characteristics are also consistent with the experimentally measured divertor probe profiles within the scatter of the data.

The simulations conducted within this study do not include cross-field drifts and currents. As a result, the focus of the simulations have been on the LFS divertor. In the unseeded simulations, the HFS radiation levels are clearly lower than measured, indicating, at least, underestimated densities and overestimated electron temperatures in the HFS divertor leg, consistent with the omission drifts. The HFS divertor leg discrepancy between the measured and predicted D_α- and total power emission are reduced with nitrogen seeding in both configurations, indicating the that the impact of drifts on the HFS/LFS-asymmetries becomes less significant in high radiation divertor conditions, where the sheath-potential driven electric fields are significantly reduced.

Acknowledgements

This work has been carried out within the framework of the EUROfusion Consortium and has received funding from the Euratom research and training programme 2014-2018 under grant agreement No 633053. The views and opinions expressed herein do not necessarily reflect those of the European Commission.

REFERENCES

[PIPB_NF_2007_chapter1] M. Shimada, *et al. Nucl. Fusion* **47** (2007) S1 – S17

[Kukushkin_FED_2011] A.S. Kukushkin, *et al. Jour. Nucl. Mater.* **86** (2011) 2865 – 2873

[Pacher_JNM_2009] H.D. Pacher, *et al. Jour. Nucl. Mater.* **390 – 391** (2009) 259 – 262

[Loarte_PPCF_2001] A. Loarte, *et al. Plasma Phys. Control. Fusion* **43** (2001) R183 – R224

[Lipschultz_FST_2007] B. Lipschultz, *et al. Fus. Sci. Tech.* **51** (2007) 369 – 389

[Schneider_JNM_1999] R. Schneider, *et al. Jour. Nucl. Mater.* **266 – 269** (1999) 175 – 181

[Asakura_NF_1999] N. Asakura, *et al. Nucl. Fusion* **39** (1999) 1983

[Loarte_JNM_1997] A. Loarte, *et al. Jour. Nucl. Mater.* **241 – 243** (1997) 118 – 134

[Loarte_NF_1998] A. Loarte, *et al. Nucl. Fusion* **38** (1998) 3.

[Groth_JNM_2015] M. Groth, *et al. Jour. Nucl. Mater.* **463** (2015) 471 – 476.

[Simonini_CPP_1994] R. Simonini, et al., Contrib. Plasma Phys. **34** (1994) 368 – 373.

[Reiter_JNM_1992] REITER, D. Jour. Nucl. Mater. **196 – 198** (1992) 80 – 89.

[Wiesen_ITC_2006] WIESEN, S., ITC- Report,
http://www.eirene.de/e2deir_report_30jun06.pdf (2006).

[Moulton_EPS_2015] D. Moulton, *et al. Proc. of the 42nd EPS conference on Plasma Physics, Lisbon, Portugal, 22nd – 26th of June, 2015.*

[Matthews_PhysScr_2011] G.F. Matthews, *et al. Phys. Scr.* **T145** (2011) 014001

[Giroud_PPCF_2015] C. Giroud, *et al. Plasma Phys. Control. Fusion* **57** (2015) 035004

[HRTSref] M.N.A. Beurskens, *et al. Nucl. Fusion* **48** (2008) 095004.

[Libeam] M. Brix, *et al. Rec. Sci. Instrum.* **83** (2012) 10D533

[LP] R.D. Monk, *et al. Jour. Nucl. Mater.* **241 – 243** (1997) 396.

[KS3_ref] P.D. Morgan, *et al. Rev. Sci. Instrum.* **56** (1985) 862

[KT3_ref] B. A. Lomanowski, *et al. Rev. Sci. Instrum.* **85** (2014) 11E432

[boloref] A. Huber, *et al. Fusion Eng. Des.* **82** (2007) 1327

[IRTV_ref] T. Eich, *et al. Jour. Nucl. Mater.* **415** (2011) S856

[Brezinsek_JNM_2014] S. Brezinsek, *et al. Jour. Nucl. Mater.* **463** (2015) 11 – 21

[Jaervinen_JNM_2014] A. E. Jaervinen, *et al. Jour. Nucl. Mater.* **463** (2015) 135 – 142

[Eckstein_sput_2007] W. Eckstein, *et al. Sputtering by particle Bombardment,* Springer Publishing, (2007).

[ADAS_reference] H. P. Summers 1994 Atomic data and analysis structure users manual, JET-IR 06 (Abingdon:JET Joint Undertaking)

[Oberkofler_JNM_2013] M. Oberkofler, *et al. Jour. Nucl. Mater.* **438** (2013) S258 – S261

[Kallenbach_PPCF_2010] A. Kallenbach, *et al. Plasma Phys. Cont. Fusion* **52** (2010) 055002.

[Kotov_PPCF_2008] V. Kotov, *et al. Plasma Phys. Control. Fusion* **50** (2008) 105012

[Bohm] D. Bohm, *The Characteristics of Electrical Discharges in Magnetic Fields,* New York: McGraw-Hill, 1949

[Chodura] R. Chodura, *Physics of Plasma-Wall Interactions in Controlled Fusion,* New York: Plenum Press, 1986

[Stangeby] P. C. Stangeby, *The Plasma Boundary of Magnetic Fusion Devices,* IoP Publishing, 2000, ISBN 0-7503-0559-2

[Chankin_PPCF_2015] A. Chankin, *et al. Plasma Phys. Control. Fusion, submitted for publication (2015).*

[AhoMantila_NF_2015] L. Aho-Mantila, *et al. Nucl. Fusion, submitted 2015*

[Groth_NF_2015] M. Groth, *et al. Proc. of the 25th IAEA, FEC, St. Petersburg, Russia, 13. – 18. Oct. 2014.*

[Groth_JNM_2015_2] M. Groth, *et al. Jour. Nucl. Mater.*, *submitted 2015*

[Huber_JNM_2013] A. Huber, *et al. Jour. Nucl. Mater.* **438** (2013) S139-S147

[Eich_PRL_2011] T. Eich, *et al. Phys. Rev. Let.* **107** (2011) 215001

[Jaervinen_NF_2015] A. E. Jaervinen, *et al. Nucl. Fusion, submitted (2015)*

[Widdowson_PhysScr_2014] A. Widdowson, *et al. Phys. Scr.,* **T159** (2014) 014010

[Lawson_JNM_2015] K. D. Lawson, *et al. Jour. Nucl. Mater.* **463** (2015) 582 – 585

[Scarabosio_JNM_2015] A. Scarabosio, *et al. Jour. Nucl. Mater.* **463** (2015) 49 – 54.

[Kallenbach_NF_2015] A. Kallenbach, *et al. Nucl. Fusion* **55** (2015) 053026.

[Reimold_JNM_2015] F. Reimold, *et al. Jour. Nucl. Mater.* **463** (2015) 128 – 134

TABLE CAPTIONS

Table 1: Analysis of the power balance within the confined region in the investigated plasmas: 1) JET pulse number (JPN), 2) magnetic configuration, 3) deuterium and nitrogen injection rates, 4) total heating power by NBI and ICRH, 5) total radiated power inside the pedestal, 6) estimated rate of the change of the pedestal stored energy during 70 – 95% of the ELM cycles, 7) estimated power crossing the separatrix during 70 – 95% of the ELM cycles, 8) estimated ELM frequency.

FIGURE CAPTIONS

Figure 1: The poloidal magnetic equilibria of the investigated JET plasmas: black (high-triangularity, horizontal target; high-δ / HT), red (high-triangularity, vertical target; high-δ / VT). The main diagnostics used in this study are highlighted: the high resolution Thomson scattering system (HRTS [HRTSref], black line at the LFS mid-plane), the lithium beam system (Li-beam [Li beam ref], black at the top), target Langmuir probes [LP ref] (Magenta), and divertor visual spectroscopy systems [KS3_ref, KT3_ref] (black, red, and blue). The total radiated power was measured with a multiple-chord bolometer and reconstructed tomographically [boloref]. A vertical viewing infrared thermography (not shown) was used to estimate the low-field side power deposition [IRTV_ref]. Deuterium was injected into the chamber at the HFS target, while nitrogen seeded at the LFS target. The horizontal dashed line at Z = -1.2 m, represent the spatial location used to distinguish between divertor and main chamber radiation. The flux surfaces 2 cm away from the separatrix are also drawn in the SOLs.

Figure 2: Measured and predicted LFS mid-plane electron density (a), LFS target electron temperature (b), and LFS target saturation current (c) profiles in the unseeded plasmas in horizontal (black) and vertical (red) divertor configurations. The measured HRTS profiles are shifted by +1.5 cm (horizontal) and +1 cm (vertical), such that the measured separatrix electron temperature is about 100 eV, which is consistent with assuming conduction-limited SOL in an H-mode plasma in a JET-sized tokamak. The measured Li-beam profiles are shifted by -0.8 cm (horizontal) and -0.5 cm (vertical) to align the separatrix n_e with the HRTS profile. Finally, the Langmuir probe profiles are shifted by +0.5 cm (horizontal) and +0.9 cm (vertical) such that the saturation current peaks in the common SOL. The EDGE2D-EIRENE catalog folders corresponding to these simulations are given in the appendix 1a.

Figure 3: Predicted 2-D deuterium ionisation distributions in the LFS divertor leg in the horizontal (a) and vertical (b) divertor configurations. The EDGE2D-EIRENE catalog folders corresponding to these simulations are given in the appendix 1a.

Figure 4: Measured and predicted vertical (a) and horizontal (b) line integrated radiated power as seen by the JET bolometer system: red (vertical LFS divertor), black (horizontal LFS divertor), lines (EDGE2D-EIRENE), squares (experiment). The location of the X-point (XP) in the profiles is illustrated with a dashed vertical line. The EDGE2D-EIRENE catalog folders corresponding to these simulations are given in the appendix 1a.

Figure 5: Measured (squares) and predicted (lines) divertor D_α-emission. The approximate location of the X-point in the profile is illustrated with dashed lines. The EDGE2D-EIRENE catalog folders corresponding to these simulations are given in the appendix 1a.

Figure 6: a) Measured reduction of the LFS divertor peak heat flux as a function of the radiated power fraction in the investigated plasma. b) Predicted reduction of the LFS divertor peak heat flux as a function of the fraction of power crossing separatrix, P_{SOL}, radiated in the SOL. The JET pulse numbers used in the experimental plot are given in the table 1. The EDGE2D-EIRENE simulation catalog folders are given in the appendix 1a.

Figure 7: Predicted (hollow squares) LFS divertor heat flux profiles in the horizontal (a) and vertical (b) divertor geometries assuming 0 MW (black), 3 MW (blue), and 6 MW (red) of nitrogen radiation. The dashed lines represent the fits to the predicted heat flux profiles, used to obtain the divertor power spreading parameter S. The normalized divertor power spreading parameters S/f_x, as given by the fits, are given in the figures. f_x stands for the poloidal flux expansion between the LFS mid-plane and the strike-point, as given by the numerical calculation grid for the separatrix field-line: horizontal 3.4, vertical 1.6. The quality of the fits is illustrated on top of the figures. The EDGE2D-EIRENE catalog folders corresponding to these simulations are given in the appendix 1a.

Figure 8: a) Predicted reduction of the LFS peak heat flux as a function of normalized SOL radiation assuming fixed $n_{e,\,sep,\,LFS\text{-}mp} \sim 4e19\ m^{-3}$. b) Predicted reduction of the LFS peak heat flux in unseeded EDGE2D-EIRENE simulations as a function of the $n_{e,\,sep,\,LFS\text{-}mp}$. The EDGE2D-EIRENE catalog folders corresponding to these simulations are given in the appendix 1b and 1c.

Figure 9: Measured and predicted line integrated radiated power as seen by the KB5 bolometer. The upper row represents the discharges with the horizontal LFS target and the lower row discharges with the vertical LFS target. The left column represents the vertical bolometer (KB5) system and the right column the horizontal bolometer (KB5) system. Black color is used for the unseeded base case, blue for the medium seeding rate and red for the high seeding rate plasmas. EDGE2D-EIRENE predictions are illustrated with solid lines, whereas the experimental data points are illustrated with squares. The EDGE2D-EIRENE catalog folders corresponding to these simulations are given in the appendix 1a.

Figure 10: Predicted 2-D radiation distribution in the divertor for the EDGE2D-EIRENE solutions compared to the measured bolometer signals in Fig. 7. The EDGE2D-EIRENE catalog folders corresponding to these simulations are given in the appendix 1a.

Figure 11: Predicted 2-D electron temperature contours in the divertor for the EDGE2D-EIRENE solutions compared to the measured bolometer signals in Fig. 7. The EDGE2D-EIRENE catalog folders corresponding to these simulations are given in the appendix 1a.

Figure 12: Measured (dots) and predicted (lines) LFS target electron temperature (a) and saturation current (b) distributions with increasing levels nitrogen seeding (unseeded/black, mid-N_2/blue, high-N_2/red) for the horizontal (upper row) and vertical (lower row) LFS divertor target configurations. The EDGE2D-EIRENE catalog folders corresponding to these simulations are given in the appendix 1a.

Figure 13: Predicted 2-D deuterium ionization distribution in the divertor for the EDGE2D-EIRENE solutions compared to the measured LFS target particle fluxes in fig. 12b. The EDGE2D-EIRENE catalog folders corresponding to these simulations are given in the appendix 1a.

Figure 14: Measured (squares) and predicted (solid lines) divertor D_α-emission distribution as seen by the JET divertor spectrometer (KS3) (fig. 1) for the cases compared to the LFS target probe profiles in the figure 10: a) horizontal LFS target, b) vertical LFS target. The estimated location of the X-point in the profile is illustrated with the dashed vertical line. The EDGE2D-EIRENE catalog folders corresponding to these simulations are given in the appendix 1a.

Figure 15: Measured (a) and predicted (b) evolution of the pedestal electron density, $n_{e,\,ped}$, as a function of the radiative power fraction (a) and SOL radiation fraction (b), $P_{rad,SOL}/P_{SOL.}$ c) Predicted deuterium ionization source inside the separatrix. d) Predicted total pressure at the LFS mid-plane separatrix and at the LFS strike point. Black color is used for the horizontal LFS target cases and red represents the vertical LFS target cases. The experimental data points and simulations are illustrated in two figures with different x-axis due to the same reason as in the figure 6. The arrows within the experimental data points illustrate the trend of the data with increasing nitrogen injection. The EDGE2D-EIRENE catalog folders corresponding to these simulations are given in the appendix 1a.

Figure 16: Predicted poloidal profiles of neutral deuterium flux crossing the separatrix in the unseeded base case (a), medium nitrogen seeding case (b) and high nitrogen seeding case (c). The EDGE2D-EIRENE catalog folders corresponding to these simulations are given in the appendix 1a.

TABLES

Table 1.

JPN	**Configuration**	**Φ_{D2} / Φ_{N2} (1e22 e/s)**	**P_{in}:NBI/ICRH (MW)**	**P_{rad}^{core} (ρ < 0.95)**	**dW^{ped}/dt (MW)**	**$P_{SOL}^{inter\text{-}ELM}$ (MW)**	**f_{ELM} (Hz)**
82806	HT3R	2.8 / 0	16 / 0	1.5	6.7 +/- 1.6	7.8 +/- 1.6	~ 15
85406	HT3R	3.1 / 0	16 / 0	1.7	6.0 +/- 1.4	8.3 +/- 1.4	~ 15
82812	HT3R	2.7 / 2.4	16 / 0	2.9	3.2 +/- 1.3	9.9 +/- 1.3	~ 15
82811	HT3R	2.8 / 3.6	16 / 0	2.6	4.7 +/- 1.2	8.7 +/- 1.2	~ 40
85408	HT3R	2.6 / 3.4	16 / 3	4.3	5.2 +/- 1.5	9.5 +/- 1.5	~ 30
85269	HTVT	2.3 / 0	16 / 4	3.3	6.8 +/- 1.2	9.9 +/- 1.2	~ 15
85272	HTVT	2.1 / 2.0	16 / 4	4.6	4.5 +/- 2.6	10.9 +/- 2.6	~ 50
85274	HTVT	2.1 / 3.5	16 / 4	3.7	5.9 +/- 4.0	10.4 +/- 4.0	~ 70

FIGURES

Figure1.

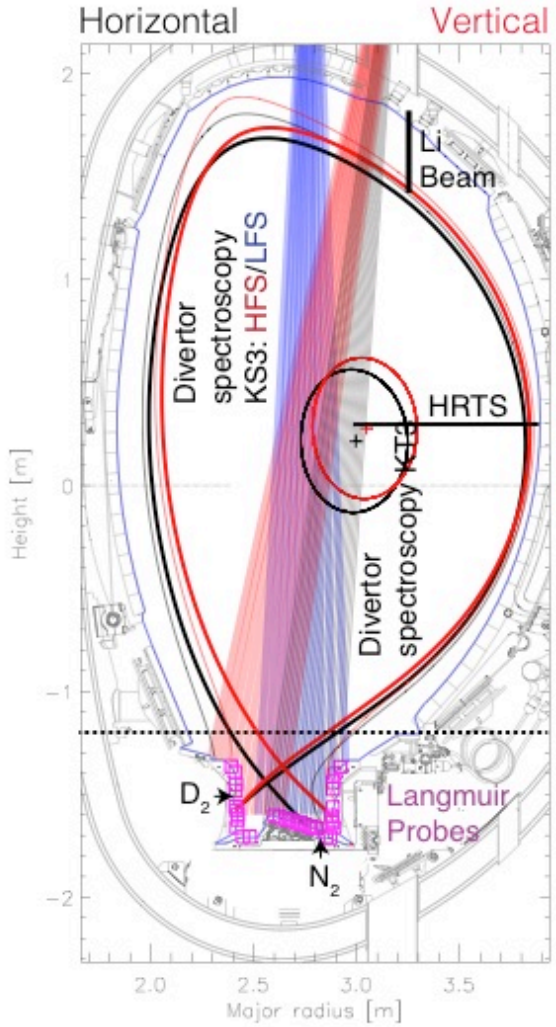

Figure 2.

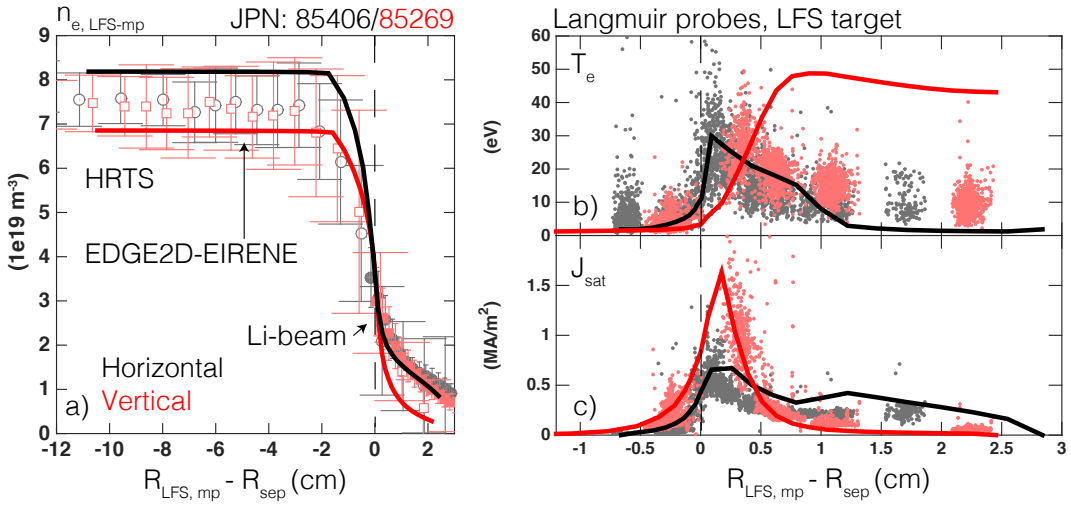
n e, LFS-mp
JPN: 85406/85269
(1e19 m-3)
HRTS
EDGE2D-EIRENE
Li-beam
Horizontal
a) Vertical
R LFS, mp - R sep (cm)
Langmuir probes, LFS target
T e
(eV)
b)
J sat
(MA/m2)
c)
R LFS, mp - R sep (cm)

Figure 3.

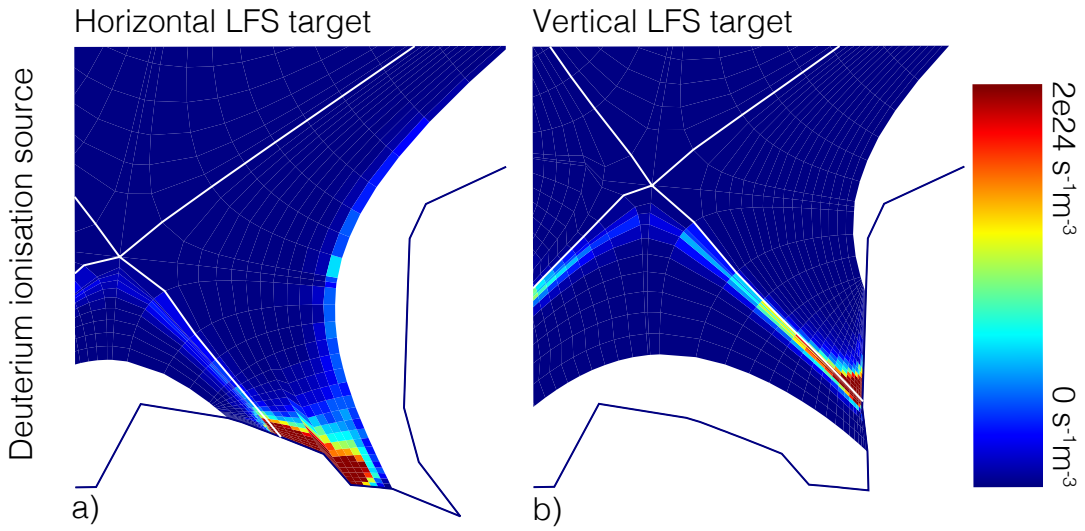
Horizontal LFS target
Vertical LFS target
Deuterium ionisation source
a)
b)
2e24 s-1m-3
0 s-1m-3

Figure 4.

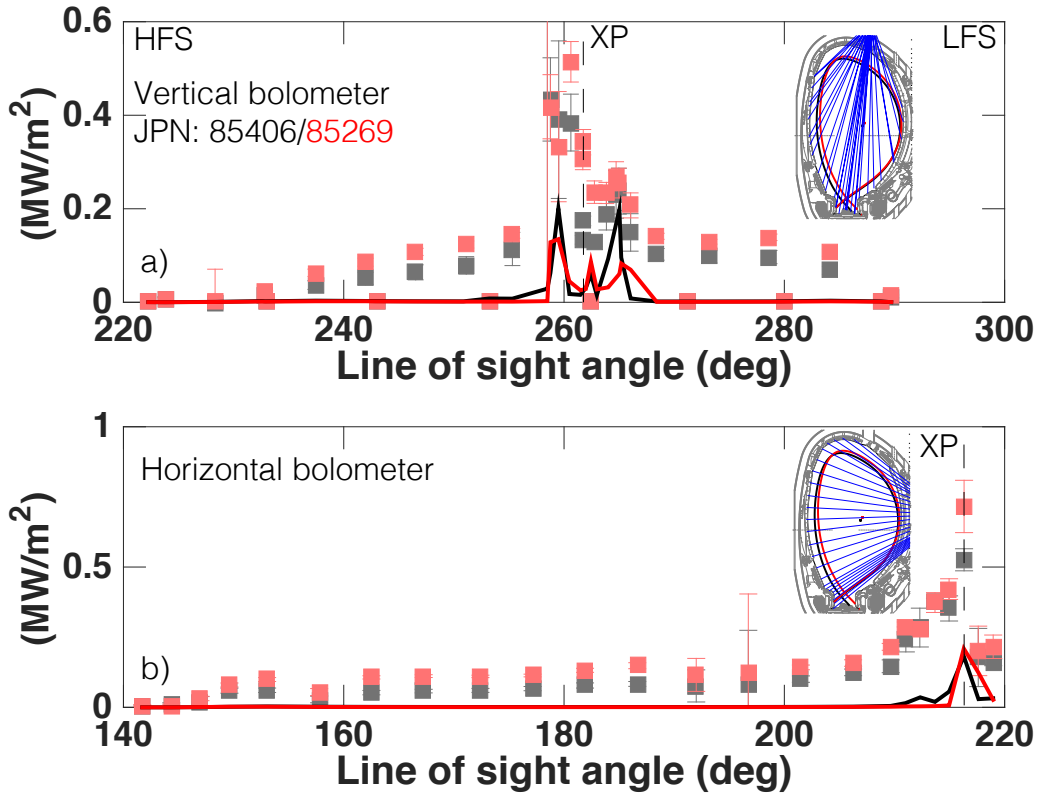
HFS
XP
LFS
Vertical bolometer
JPN: 85406/85269
a)
(MW/m2)
0.6
0.4
0.2
0
220
240
260
280
300
Line of sight angle (deg)
Horizontal bolometer
XP
b)
(MW/m2)
1
0.5
0
140
160
180
200
220
Line of sight angle (deg)

Figure 5.

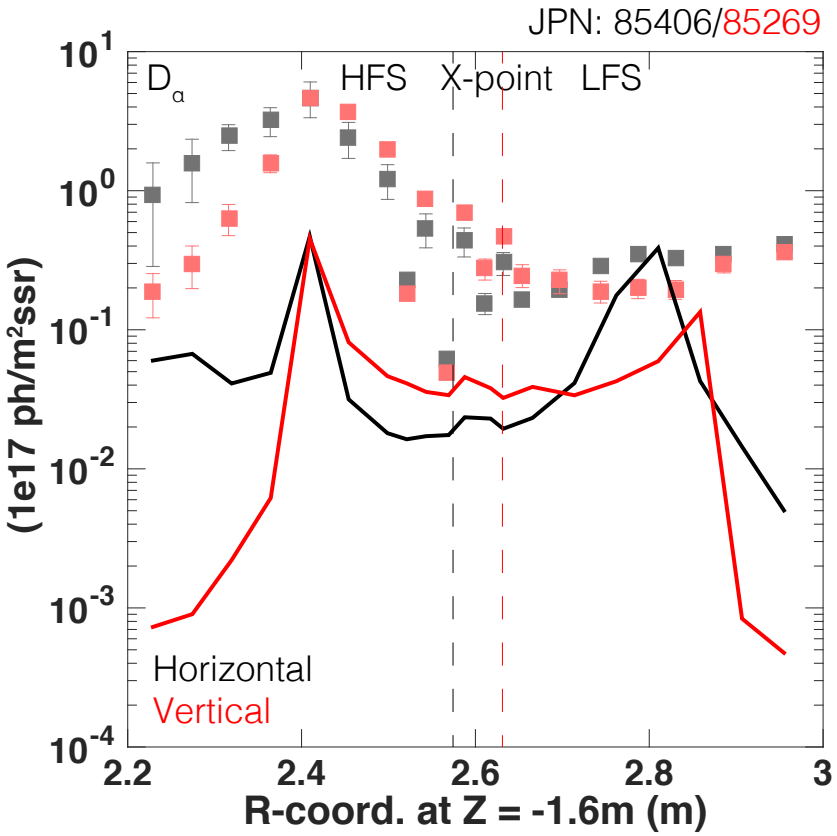
JPN: 85406/85269
D_α
HFS
X-point
LFS
10^{1}
10^{0}
10^{-1}
10^{-2}
10^{-3}
10^{-4}
(1e17 ph/m²ssr)
Horizontal
Vertical
2.2
2.4
2.6
2.8
3
R-coord. at Z = -1.6m (m)

Figure 6.

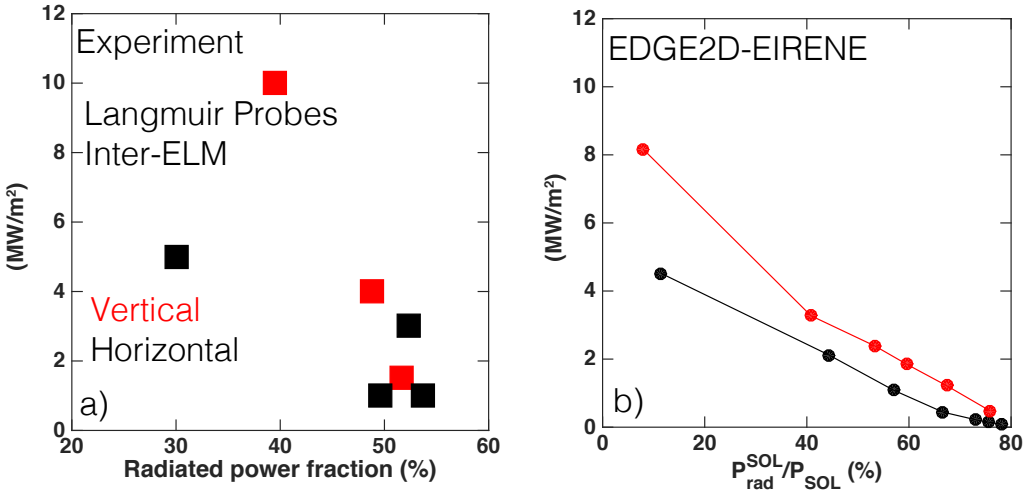
Experiment
Langmuir Probes
Inter-ELM
Vertical
Horizontal
a)
(MW/m²)
Radiated power fraction (%)
EDGE2D-EIRENE
b)
(MW/m²)
P^SOL_rad/P_SOL (%)

Figure 7.

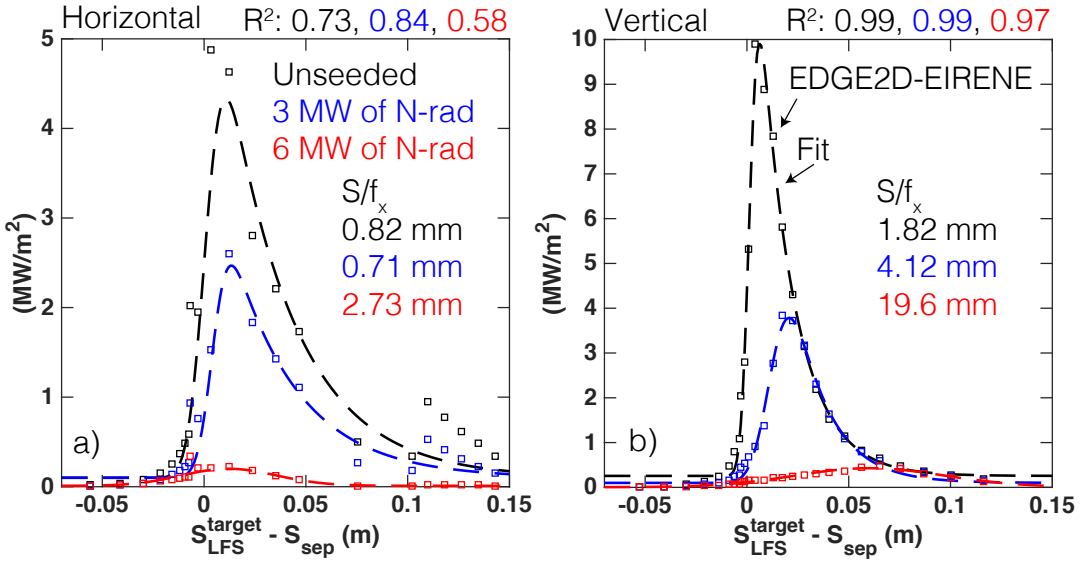
Horizontal
R²: 0.73, 0.84, 0.58
Unseeded
3 MW of N-rad
6 MW of N-rad
S/f_x
0.82 mm
0.71 mm
2.73 mm
a)
(MW/m²)
S^target_LFS - S_sep (m)
Vertical
R²: 0.99, 0.99, 0.97
EDGE2D-EIRENE
Fit
S/f_x
1.82 mm
4.12 mm
19.6 mm
b)
(MW/m²)
S^target_LFS - S_sep (m)

Figure 8.

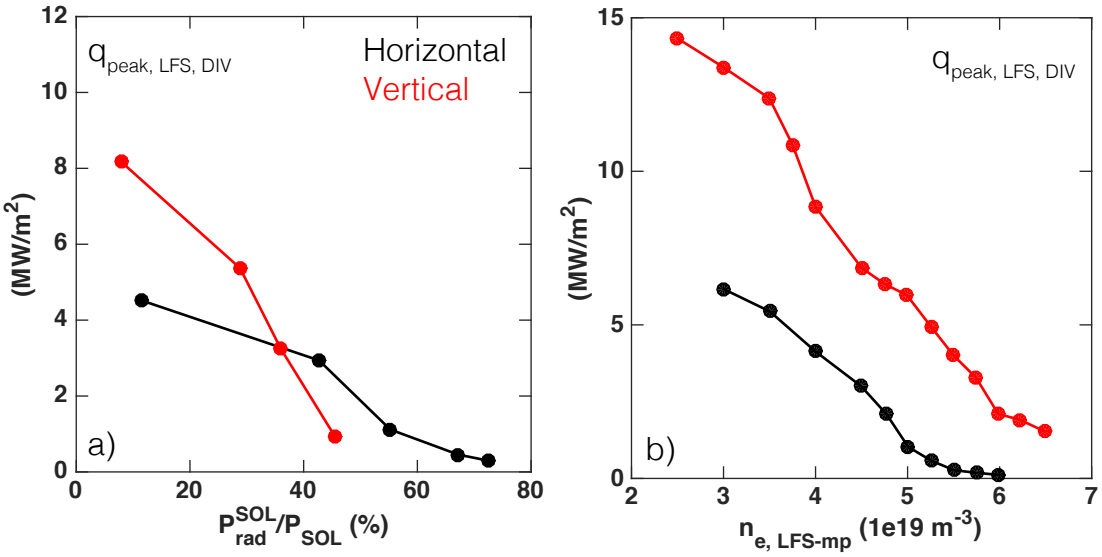
q peak, LFS, DIV
Horizontal
Vertical
(MW/m2)
a)
P SOL rad /P SOL (%)
q peak, LFS, DIV
(MW/m2)
b)
n e, LFS-mp (1e19 m-3)

Figure 9.

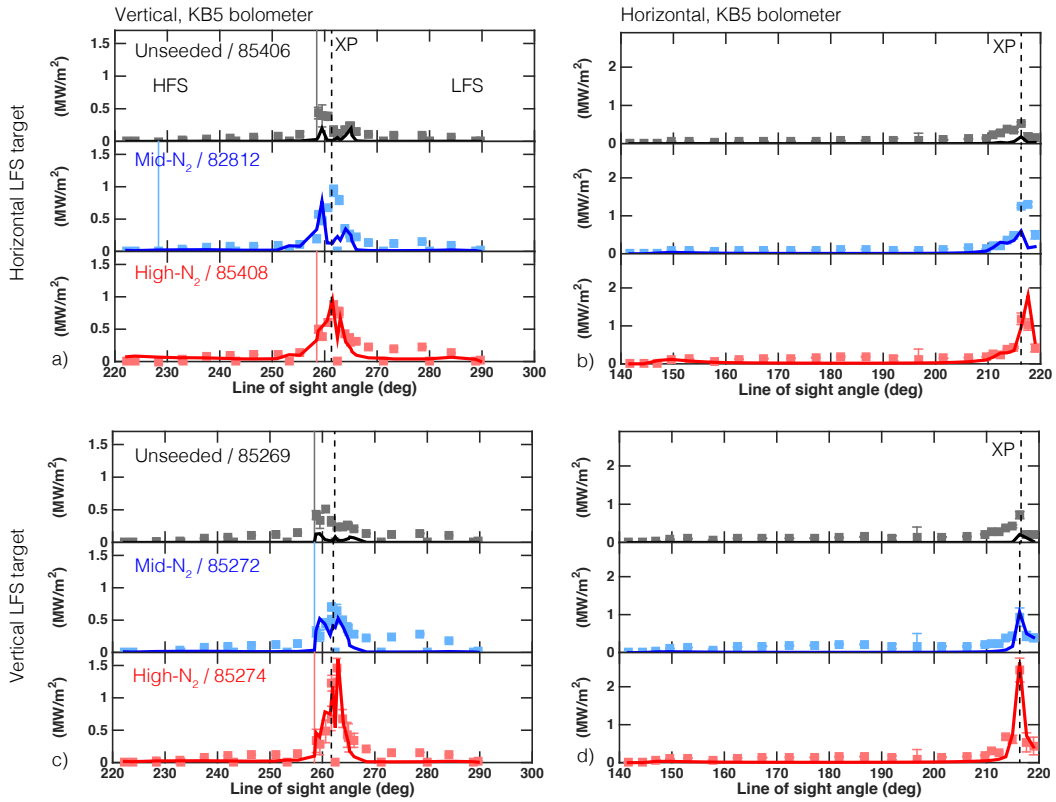
Vertical, KB5 bolometer
Horizontal, KB5 bolometer
Horizontal LFS target
Vertical LFS target
Unseeded / 85406
Mid-N2 / 82812
High-N2 / 85408
Unseeded / 85269
Mid-N2 / 85272
High-N2 / 85274
XP
HFS
LFS
(MW/m2)
Line of sight angle (deg)
a)
b)
c)
d)

Figure 10.

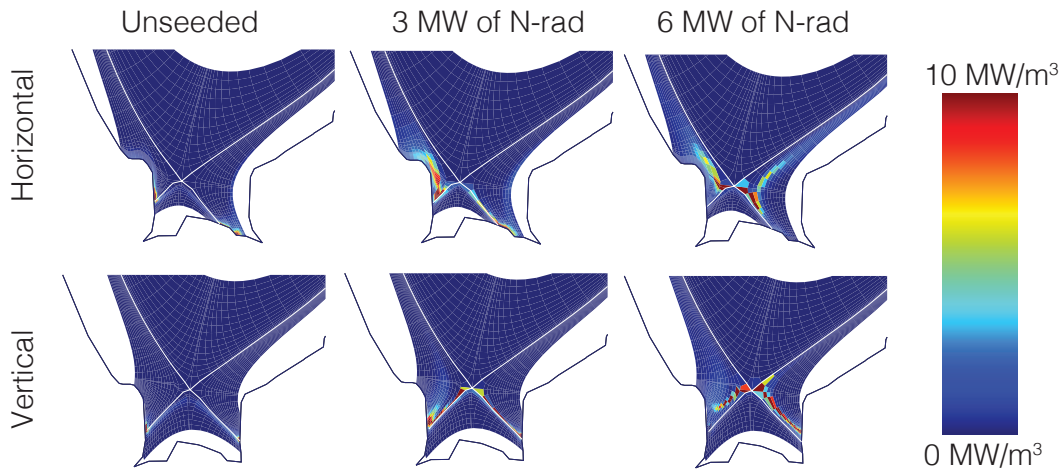
Unseeded
3 MW of N-rad
6 MW of N-rad
Horizontal
Vertical
10 MW/m3
0 MW/m3

Figure 11.

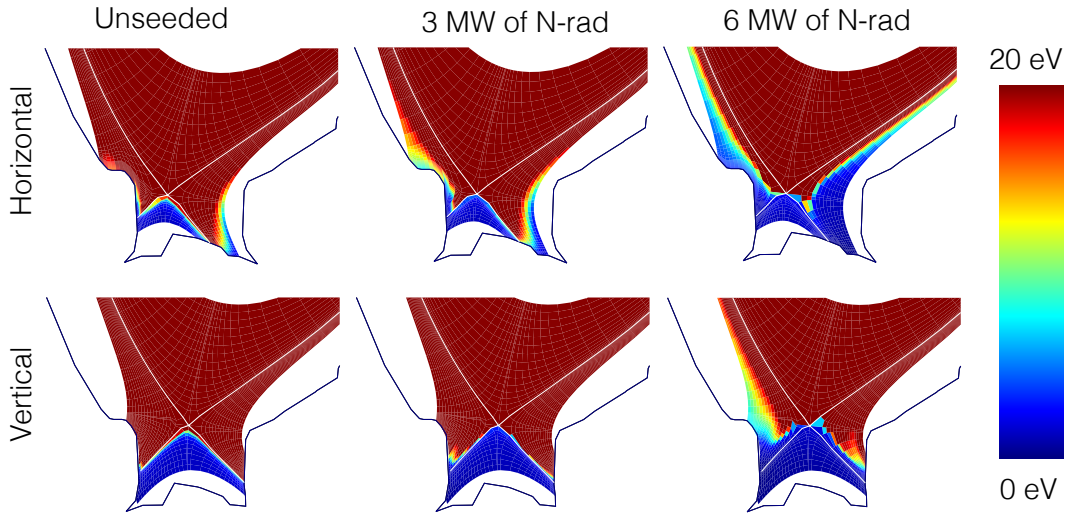
Unseeded
3 MW of N-rad
6 MW of N-rad
Horizontal
Vertical
20 eV
0 eV

Figure 12.

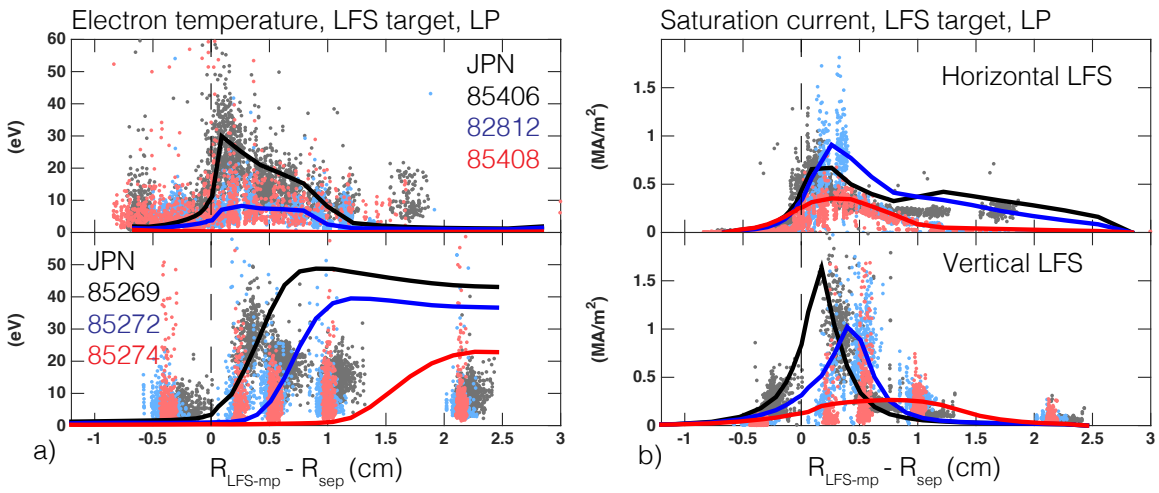
Electron temperature, LFS target, LP
JPN
85406
82812
85408
JPN
85269
85272
85274
(eV)
a)
R_LFS-mp - R_sep (cm)
Saturation current, LFS target, LP
Horizontal LFS
Vertical LFS
(MA/m²)
b)
R_LFS-mp - R_sep (cm)

Figure 13.

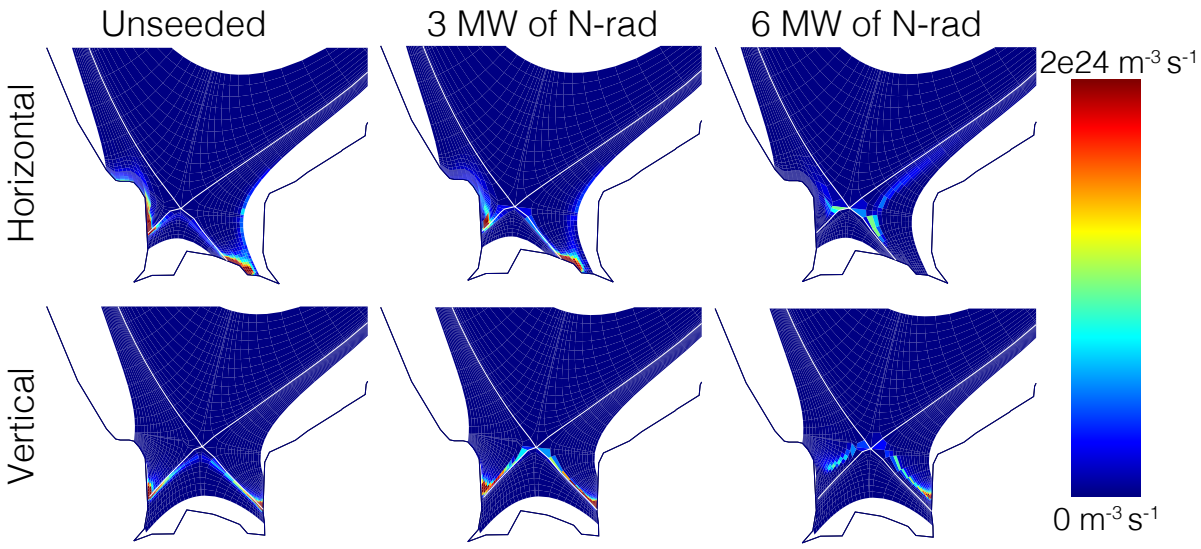
Unseeded
3 MW of N-rad
6 MW of N-rad
Horizontal
Vertical
2e24 m-3 s-1
0 m-3 s-1

Figure 14.

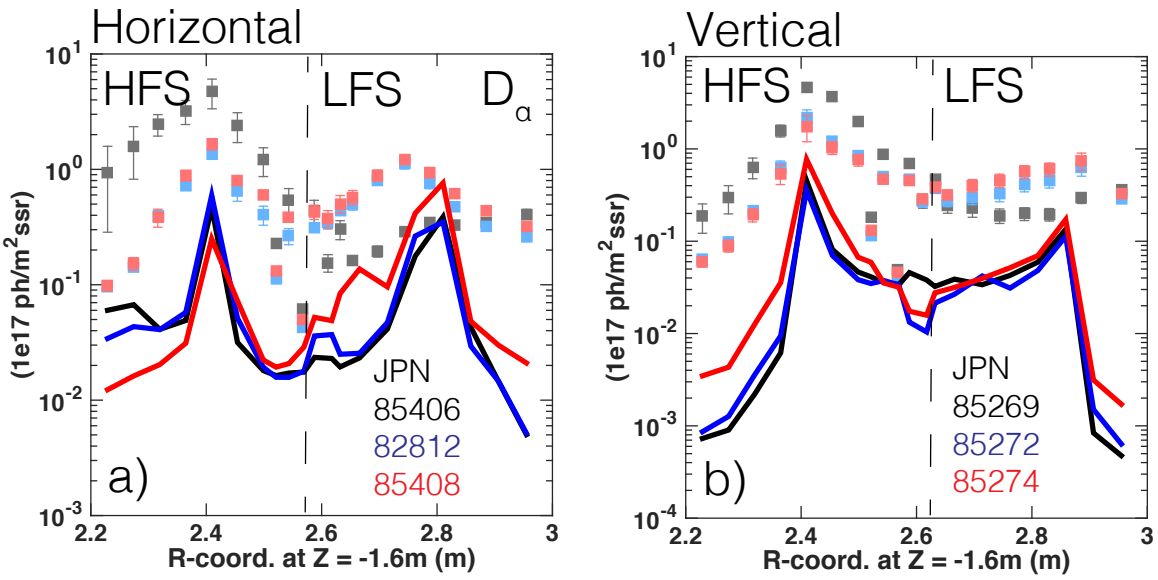
Horizontal
HFS
LFS
D_α
JPN
85406
82812
85408
a)
(1e17 ph/m^{2}ssr)
R-coord. at Z = -1.6m (m)
Vertical
HFS
LFS
JPN
85269
85272
85274
b)
(1e17 ph/m^{2}ssr)
R-coord. at Z = -1.6m (m)

Figure 15.

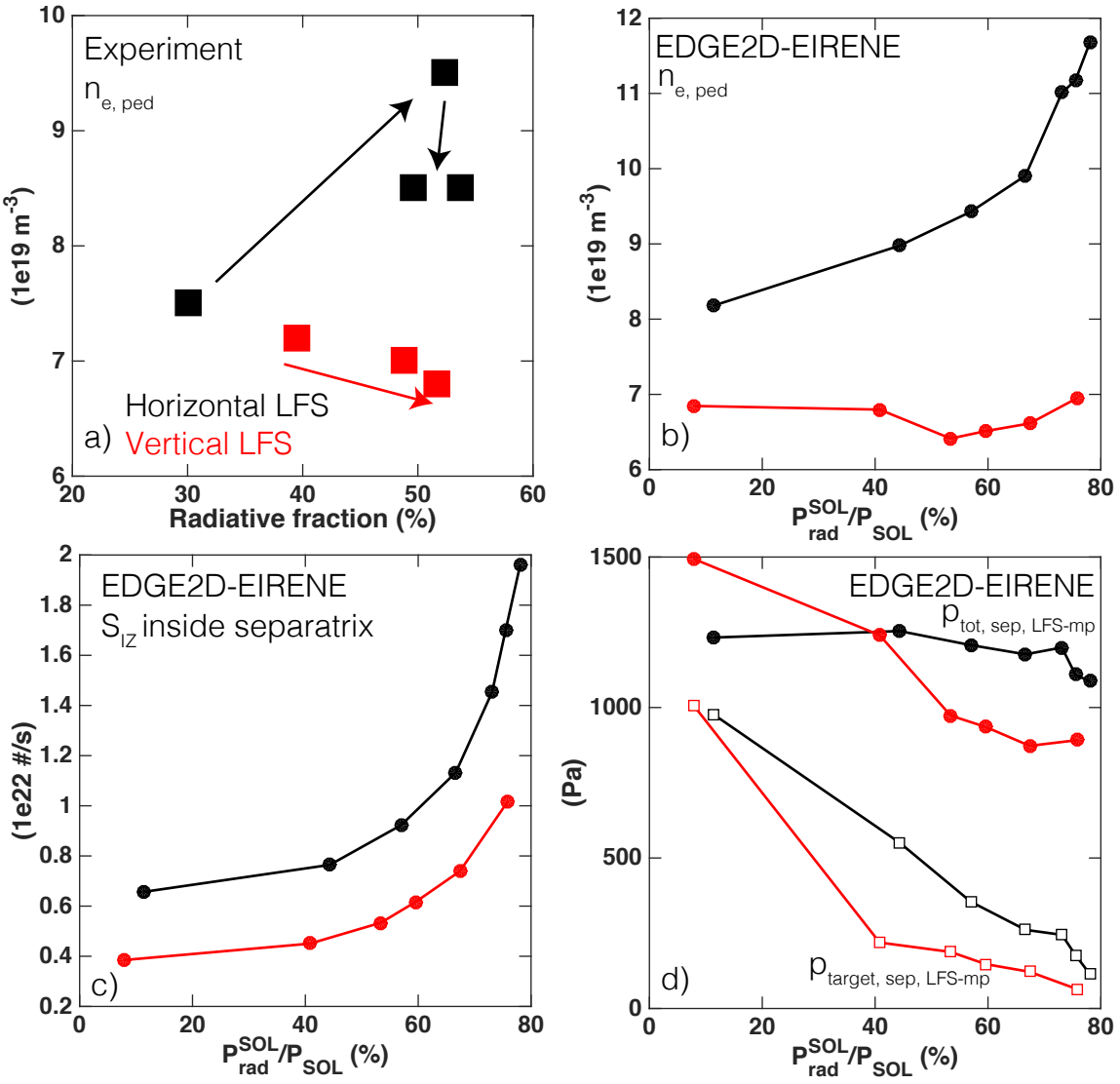
Experiment
n e, ped
Horizontal LFS
a) Vertical LFS
(1e19 m-3)
Radiative fraction (%)
EDGE2D-EIRENE
n e, ped
b)
(1e19 m-3)
P rad SOL/P SOL (%)
EDGE2D-EIRENE
S IZ inside separatrix
c)
(1e22 #/s)
P rad SOL/P SOL (%)
EDGE2D-EIRENE
p tot, sep, LFS-mp
p target, sep, LFS-mp
d)
(Pa)
P rad SOL/P SOL (%)

Figure 16.

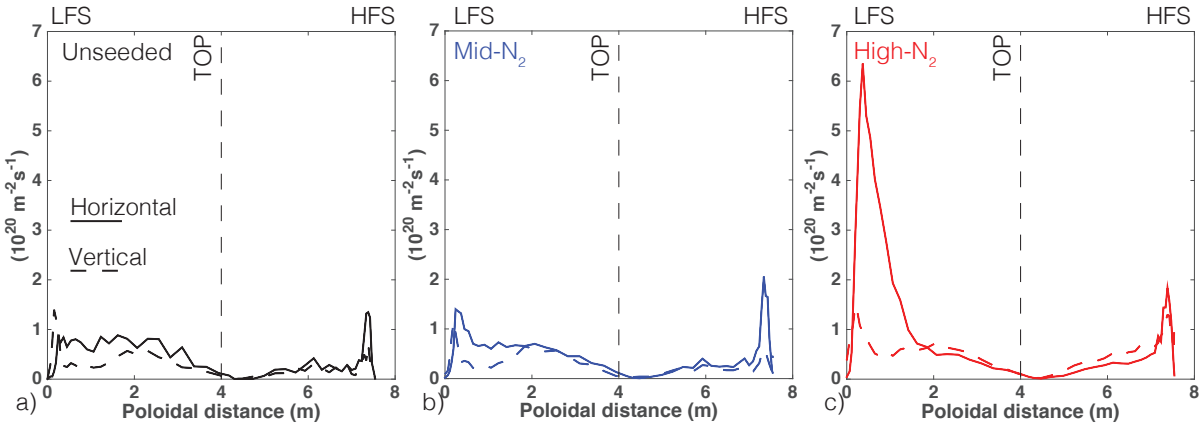
LFS
HFS
Unseeded
TOP
Horizontal
Vertical
(10^20 m^-2 s^-1)
Poloidal distance (m)
a)
Mid-N2
b)
High-N2
c)

Appendix 1a. The EDGE2D-EIRENE catalog folders representing the nitrogen injection scans with floating $n_{e,\,sep,\,LFS\text{-}MP}$. All the simulations are in the subfolder 'ajarvin/edge2d/jet/'. The simulation cases illustrated with the red color reach a MARFE-like radiation condensation formation at the X-point and do not reach a converged state within the convergence criterions used in this study.

N-radiation level (MW)	Horizontal LFS target	Vertical LFS target
0	83357/feb0115/seq#1	85274/mar2415/seq#2
3	83357/jan2414/seq#10	85274/mar1715/seq#2
4	83357/jan2415/seq#14	85274/mar2415/seq#3
4.5		85274/apr2115/seq#15
5	83357/jan2415/seq#17	85274/jun0415/seq#1
5.5	83357/jan2515/seq#5	
5.75	83357/jan2515/seq#6	
6	83357/jun1815/seq#1	85274/jun2415/seq#3
7	83357/jun0115/seq#12	85247/jul0315/seq#1

Appendix 1b. The EDGE2D-EIRENE catalog folders representing the nitrogen injection scans with feed back controlled $n_{e,\,sep,\,LFS\text{-}MP} \sim$ 4e19 m^{-3}. All the simulations are in the subfolder 'ajarvin/edge2d/jet/'.

N-radiation level (MW)	Horizontal LFS target	Vertical LFS target
2		85274/aug2815/seq#1
2.5		85274/aug2815/seq#2
3	83357/aug0615/seq#1	85274/sep1115/seq#2
4	83357/jul2415/seq#1	
5	83357/jul2415/seq#2	
5.5	83357/jul2515/seq#1	

Appendix 1c. The EDGE2D-EIRENE catalog folders representing the unseeded density scans. All the simulations are in the subfolder 'ajarvin/edge2d/jet/'.

$n_{e,\,sep,\,LFS\text{-}MP}$ (1e19 m^{-3})	Horizontal	Vertical
2.50		85274/mar0715/seq#4
3.00	83357/may0115/seq#1	85274/mar0715/seq#1
3.50	83357/may0115/seq#2	85274/mar0715/seq#2
3.75		85274/mar0715/seq#8
4.00	83357/may0115/seq#3	85274/mar1215/seq#1
4.50	83357/may0115/seq#4	85274/mar1715/seq#1
4.75	83357/may0115/seq#5	85274/mar1715/seq#3
5.00	83357/may0215/seq#1	85274/mar1315/seq#4
5.25	83357/may0215/seq#2	85274/mar2015/seq#1
5.50	83357/may0415/seq#1	85274/mar2015/seq#2
5.75	83357/may0215/seq#3	85274/mar2015/seq#3
6.00	83357/may0215/seq#4	85274/mar2215/seq#2
6.25		85274/mar2215/seq#3
6.50		85274/mar2715/seq#1